MULTISCALE MODEL. SIMUL.
Vol. 22, No. 3, pp. 1097–1135

MULTISCALE APPROACH FOR VARIATIONAL PROBLEM JOINT DIFFEOMORPHIC IMAGE REGISTRATION AND INTENSITY CORRECTION: THEORY AND APPLICATION*

PENG CHEN†, KE CHEN‡, HUAN HAN§, AND DAOPING ZHANG¶

Abstract. Image registration matches the features of two images by minimizing the intensity difference, so that useful and complementary information can be extracted from the mapping. However, in real life problems, images may be affected by the imaging environment, such as varying illumination and noise during the process of imaging acquisition. This may lead to the local intensity distortion, which makes it meaningless to minimize the intensity difference in the traditional registration framework. To address this problem, we propose a variational model for joint image registration and intensity correction. Based on this model, a related greedy matching problem is solved by introducing a multiscale approach for joint image registration and intensity correction. An alternating direction method (ADM) is proposed to solve each multiscale step, and the convergence of the ADM method is proved. For the numerical implementation, a coarse-to-fine strategy is further proposed to accelerate the numerical algorithm, and the convergence of the proposed coarse-to-fine strategy is also established. Some numerical tests are performed to validate the efficiency of the proposed algorithm.

Key words. image registration, diffeomorphism, multiscale, coarse to fine, multiresolution, multigrid

MSC codes. 68U10, 94A08, 65K10, 65M12

DOI. 10.1137/23M155952X

1. Introduction.

Image registration is to match the features of two images by keeping one image (target image) unchanged and deforming the other image (floating image). By comparing the deformed image with the target image, one can extract useful information from intensity difference. This is a fundamental process for image fusion and medical analysis. For an overview of image registration and related joint problems, one can refer to [1, 3, 5, 6, 7, 10, 14, 15, 24, 25, 34] for details.

Without loss of generality, in this paper, we mainly focus on 2D image registration, which is stated in the following way. For some bounded domain $\Omega \subset \mathbb{R}^2$, given two

*Received by the editors March 17, 2023; accepted for publication (in revised form) May 15, 2024; published electronically August 29, 2024. All the authors contributed equally to this work.
https://doi.org/10.1137/23M155952X
Funding: The work of the first author was supported in part by Natural Science Foundation of Hubei Province of China grant 2024AFB730. The work of the second author was supported in part by Engineering and Physical Sciences Research Council grant EP/N014499/1. The work of the third author was supported in part by National Natural Science Foundation of China grant 11901443 and Natural Science Foundation of Hubei Province of China 2022CFB379. The work of the fourth author was supported in part by National Natural Science Foundation of China grant 12201320 and Fundamental Research Funds for the Central Universities, Nankai University grants 63221039 and 63231144.

†College of Science, China Three Gorges University, Yichang 443002, People's Republic of China (pengchen729@sina.com).
‡Department of Mathematics and Statistics, University of Strathclyde, Glasgow, G1 1XH, United Kingdom, and Centre for Mathematical Imaging Techniques, University of Liverpool, Liverpool L69 7ZL, United Kingdom (K.Chen@strath.ac.uk).
§Corresponding author. Department of Mathematics, Wuhan University of Technology, Wuhan 430070, People's Republic of China (hanhuan11@whut.edu.cn).
¶School of Mathematical Sciences and LPMC, Nankai University, Tianjin 300071, People's Republic of China (daopingzhang@nankai.edu.cn).

images $T(\mathbf{x}), D(\mathbf{x}) : \mathbf{x} \in \Omega \to \mathbb{R}$, the goal of image registration is to find a mapping $\boldsymbol{\varphi}(\mathbf{x}) : \mathbf{x} \in \Omega \to \Omega$ such that $T \circ \boldsymbol{\varphi}(\cdot)$ looks like $D(\cdot)$ as much as possible. For each $\mathbf{x} \in \Omega$, $\boldsymbol{\varphi}(\mathbf{x})$ can be divided into the identity part $\mathbf{x}$ and the displacement $\mathbf{u}(\mathbf{x})$, i.e., $\boldsymbol{\varphi}(\mathbf{x}) \triangleq \mathbf{x} + \mathbf{u}(\mathbf{x})$. Based on this assumption, the mono-modality image registration problem is formulated as follows:

$$\min_{\mathbf{u} \in \mathcal{A}} \ \lambda S(\mathbf{u}) + \mu R(\mathbf{u}), \tag{1.1}$$

where the fidelity is

$$S(\mathbf{u}) = \int_{\Omega} (T(\mathbf{x} + \mathbf{u}(\mathbf{x})) - D(\mathbf{x}))^2 d\mathbf{x},$$

$R(\mathbf{u})$ is a regularization to allow plausible solutions, $\mathcal{A}$ is some proper set, and the constants $\lambda, \mu > 0$ are used to balance the fidelity and regularization. For the multi-modality image registration [4, 28], the fidelity is

$$S(\mathbf{u}) = \int_{\Omega} (f_1(T(\mathbf{x} + \mathbf{u}(\mathbf{x}))) - f_2(D(\mathbf{x})))^2 d\mathbf{x},$$

where f_1, f_2 are two intensity transform functions. The problem considered in this paper lies between these two types of registration problems, because the given images appear in multimodality but the modeling must be done in mono-modality.

Although image registration has achieved enormous success, it is still a challenging task. There are two main difficulties: (I) physical mesh folding and (II) ill-poseness of greedy matching. As shown in Figure 1, physical mesh folding is a phenomenon that points from different objects are mixed mutually after doing the transformation. We can find that the essential reason for mesh folding is the non-bijection of the deformation mapping. Therefore, to eliminate mesh folding, it is necessary to guarantee that the Jacobian determinant of the deformation is larger than 0 for each pixel [13, 18, 19]. This is the so-called "orientation-preserving registration." Under this framework, some diffeomorphic image registration models have been proposed [8, 17, 18, 19, 21, 23, 27, 30, 31, 36, 39, 40]. Specifically, they can be mainly classified into three categories: (i) Using quasi-conformal/conformal theory [17, 18, 19, 21, 23, 27, 30, 31, 36, 39, 40] to control the Beltrami coefficient; (ii) constraining the solution to the set which ensures $\det(\nabla \boldsymbol{\varphi}(\mathbf{x})) > 0$ for each $\mathbf{x} \in \Omega$; (iii) introducing the stored energy function of an Ogden material [8]. For the first choice, Lam and Lui [23] introduced the quasi-conformal theory to control the mesh folding. Following this work, several models were proposed to improve the quasi-conformal model. As a supplement, Zhang and Chen [38] introduced a diffeomorphic image registration model by controlling the modulus of Beltrami coefficient smaller than 1. Han and A. Wang, Han and Z. Wang, and Han, Z. Wang, and Zhang also gave a

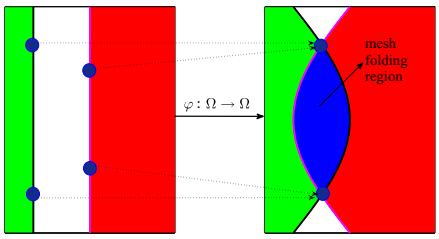

FIG. 1. *Physical mesh folding caused by the deformation* $\boldsymbol{\varphi}$.

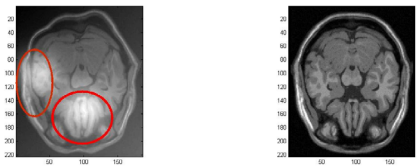

(a) $T(\cdot)$ (b) $D(\cdot)$

FIG. 2. *Local varying illumination in MRI image pair.*

series of 2D/3D diffeomorphic image registration models and algorithms by restricting $\mathbf{u}$ into the 2D/3D conformal set (Cauchy–Riemann constraint) [17, 18, 19, 21]. Particularly, in [40], Zhang et al. proposed a unifying framework for n-dimensional quasi-conformal mappings by minimizing the distance between the expected solution and the conformal set. This framework is essentially equivalent to the relaxed form of the Cauchy–Riemann constraint (section 2 in [18]) in some sense. For the second choice, Zhang, Chen, and Yu [42] proposed a diffeomorphic image registration model by restricting the deformation $\boldsymbol{\varphi}$ into a set which ensures $\det(\nabla\boldsymbol{\varphi}(\mathbf{x})) > 0$ for each $\mathbf{x} \in \Omega$. For the third choice, Debroux, Le Guyader, and Vese [8] established a framework of variational methods and hyperelasticity by viewing the shapes to be matched as Ogden materials. Though more restrictive compared with quasi-conformal mappings, the Cauchy–Riemann equation (conformal mapping) [18] is still selected as the constraint in this paper by the following reasons: it preserves the topological structure of tissue and provides a much simpler constraint (linear constraint) for diffeomorphic mappings, which further makes it possible for the mathematical analysis of the proposed model (i.e., address the greedy matching [20, 21]).

The above-mentioned works are all based on the assumption that no intensity distortion (i.e., illumination and noise) occurs during the process of imaging acquisition. For example, in Figure 2, the locally varying illumination occurs inside the region of the floating image $T(\cdot)$, and there is no illumination in the target image $D(\cdot)$. This leads to the intensity distortion for these two regions. In this case, models such as (1.1), by treating T, D as mono-modal images, fail to do the registration. It is meaningless for latter applications, such as image fusion and image analysis, even if the sketch of the two objects are exactly matched as a multimodal problem. Therefore, it is necessary to introduce some intensity correction steps during or after image registration. For this purpose, some variational models for joint image registration and intensity correction are proposed [29, 33]. By introducing the additive and multiplicative bias fields for intensity correction simultaneously, the relationship between the true image $I^*(\mathbf{x}) = I_c(\mathbf{x})$ and the obtained image $I(\mathbf{x})$ is formulated as

$$I(\mathbf{x}) = m(\mathbf{x})I^*(\mathbf{x}) + s(\mathbf{x}),$$

where $s(\mathbf{x}) : \mathbf{x} \in \Omega \to \mathbb{R}$ and $m(\mathbf{x}) : \mathbf{x} \in \Omega \to \mathbb{R}^+$ are additive and multiplicative bias fields, respectively. Based on the assumption that there is no bias in target image $D(\cdot)$, Theljani and Chen [33] proposed a model for joint image registration and intensity correction,

$$\min_{\mathbf{u},m,s} \lambda S_c(\mathbf{u}, m, s) + \mu R(\mathbf{u}, m, s), \tag{1.2}$$

where the fidelity is

$$S_c(\mathbf{u}, m, s) = \int_\Omega (m(\mathbf{x})D(\mathbf{x}) + s(\mathbf{x}) - T(\mathbf{x} + \mathbf{u}(\mathbf{x})))^2 d\mathbf{x},$$

and $R(\mathbf{u}, m, s)$ is a regularization on $\mathbf{u}, m$, and s. Viewing the solution of the variational model (1.2) as a Nash game equilibrium, a novel numerical algorithm for joint image registration and intensity correction is also devised in [33]. However, the above-mentioned mesh folding (difficulty I) is not constrained, and the game solution is a "perturbed solution," not a minimizer, of the original variational functional. The other works on joint image registration and intensity correction can be found in [11, 12].

The ultimate goal for joint image registration and intensity correction is to find the minimizer of the cost functional $S_c(\mathbf{u}, m, s)$. However, (1.2) aims to find the minimizer of $\lambda S_c(\mathbf{u}, m, s) + \mu R(\mathbf{u}, m, s)$. This raises a question of whether or not one can find the global minimizer of $S_c(\mathbf{u}, m, s)$ on some proper space without any prior estimate for $\mathbf{u}, m, s$? This is the so-called "greedy matching." Concerning this problem (difficulty II), Han, Wang, and Zhang [20, 21] gave an answer in the case of $m(\mathbf{x}) \equiv 1$, $s(\mathbf{x}) \equiv 0$, and T, D having no bias (i.e., image registration without intensity correction) by introducing a multiscale approach and proved the equivalence between the proposed multiscale approach and "greedy matching" with some suitable parameters. For the general case, to the best of our knowledge, there seems to be no results. Hence, motivated by [20, 21], in this paper, we aim to extend the work [20] to the case that m, s belong to some specific Banach spaces. For this purpose, we propose the following variational model for joint diffeomorphic image registration and intensity correction:

$$\min_{\mathbf{u}\in\mathcal{A}(\Omega)\setminus\mathcal{B}_\varepsilon(\Omega), m\in\mathcal{C}_\Omega, s\in SV_0(\Omega)} J(\mathbf{u}, m, s) := \lambda S_{lc}(\mathbf{u}, m, s) + \mu R(\mathbf{u}, m, s), \tag{1.3}$$

where

$$S_{lc}(\mathbf{u}, m, s) = \int_\Omega (m(\mathbf{x}) + \ln D(\mathbf{x}) - \ln(T(\mathbf{x} + \mathbf{u}(\mathbf{x})) - s(\mathbf{x})))^2 d\mathbf{x},$$
$$R(\mathbf{u}, m, s) = R_1(\mathbf{u}) + R_2(m) + R_3(s),$$

and

$$R_1(\mathbf{u}) = \int_\Omega |\nabla^\alpha \mathbf{u}(\mathbf{x})|^2 d\mathbf{x}, \quad R_2(m) = \int_\Omega |\nabla m(\mathbf{x})| d\mathbf{x}, \quad R_3(s) = \int_\Omega |\nabla s(\mathbf{x})| d\mathbf{x}.$$

Note that here and in what follows, we assume that two images T, D map Ω onto the interval $[\kappa, \overline{M}] \subset \mathbb{R}^+$ for some $\overline{M} > \kappa > 0$. In addition, for the purpose of eliminating mesh folding, $\mathbf{u}$ is constrained into the set $\mathcal{A}(\Omega) \setminus \mathcal{B}_\varepsilon(\Omega)$, where $\mathcal{A}(\Omega)$ and $\mathcal{B}_\varepsilon(\Omega)$ are defined by

$$\mathcal{A}(\Omega) = \left\{ \mathbf{u} = (u_1, u_2)^T \in [H_0^\alpha(\Omega)]^2 : \frac{\partial u_1}{\partial x_1} = \frac{\partial u_2}{\partial x_2}, \frac{\partial u_1}{\partial x_2} = -\frac{\partial u_2}{\partial x_1} \right\} \tag{1.4}$$

and

$$\mathcal{B}_\varepsilon(\Omega) = \{ \mathbf{u} = (u_1, u_2)^T \in \mathcal{A}(\Omega) : \det(\nabla(\mathbf{x} + \mathbf{u}(\mathbf{x}))) < \varepsilon \}, \tag{1.5}$$

for some given fractional-order α ($\alpha > 2$), small $\varepsilon > 0$, and where $H_0^\alpha(\Omega)$ is a fractional-order Sobelev space [16]. To control the intensity bias in practice, the multiplicative bias field m is constrained into the set

$$\mathcal{C}_\Omega = \{ m \in BV_0(\Omega) : K_1 \le m \le K_2 \}, \tag{1.6}$$

for some given K_1, K_2, and the additive bias field s is constrained into the set

$$SV_0(\Omega) = \{s \in BV_0(\Omega) : s(\mathbf{x}) < \kappa - \kappa_0 \text{ for } \forall \mathbf{x} \in \Omega\},$$

for some $\kappa > \kappa_0 > 0$ to ensure that $\ln(T(\mathbf{x} + \mathbf{u}(\mathbf{x})) - s(\mathbf{x}))$ is well defined. Here, $BV_0(\Omega) = \{m \in BV(\Omega) : m(\mathbf{x})|_{\mathbf{x}\in\partial\Omega} = 0\}$, and the space $BV(\Omega)$ is defined in [32].

Remark 1.1. In the proposed model (1.3), the fractional-order α is set to be greater than 2 to ensure that the first-order derivatives in $\mathcal{A}(\Omega)$ are well defined ($H_0^\alpha(\Omega) \hookrightarrow C^1(\Omega)$ for $\alpha > 2$ (Theorem 4.58 in [9])). In addition, by letting $m(\mathbf{x}) \equiv 1$ and $s(\mathbf{x}) \equiv 0$, one can notice that the model (1.2) is reduced to model (1.1), which means that model (1.2) is much more general than model (1.1).

Remark 1.2. By setting $m(\mathbf{x}) = \ln \bar{m}(\mathbf{x})$ for some positive function $\bar{m}(\mathbf{x})$, $S_{lc}(\mathbf{u}, m, s)$ from (1.2) becomes

$$S_{lc}(\mathbf{u}, m, s) = \int_\Omega \left(\ln \frac{T(\mathbf{x} + \mathbf{u}(\mathbf{x})) - s(\mathbf{x})}{\bar{m}(\mathbf{x}) D(\mathbf{x})} \right)^2 d\mathbf{x}. \tag{1.7}$$

That is, minimizing $S_{lc}(\mathbf{u}, m, s)$ in (1.3) is equivalent to minimizing $S_c(\mathbf{u}, m, s)$ in (1.2). Using (1.7) as the data fidelity for (1.3) has two advantages: (i) transforming the multiplicative bias field into the additive bias field and (ii) eliminating the positive constraint $m(\mathbf{x}) > 0$ in the definition of $S_c(\mathbf{u}, m, s)$. In addition, by using $S_{lc}(\mathbf{u}, m, s)$ as the fidelity data, the final matched image for (1.3) should be calculated as $T_c(\cdot) = \frac{T(\cdot + \mathbf{u}(\cdot)) - s(\cdot)}{e^{m(\cdot)}}$.

Remark 1.3. Similar to the model (1.2), the fidelity in (1.3) is formulated based on the assumption that the target image $D(\cdot)$ has no bias. For the situation where $T(\cdot)$ and $D(\cdot)$ are both affected by bias, two different biases (i.e., m_T, s_T and m_D, s_D) are necessary to be introduced to construct a Bi-bias fidelity $S_{lc}(\mathbf{u}, m_T, s_T, m_D, s_D)$. This situation will be considered in our forthcoming work.

Further, based on the model (1.3), in this paper, we propose a multiscale approach for joint image registration and intensity correction, which aims to find the global minimizer of $S_{lc}(\mathbf{u}, m, s)$ on $\mathcal{A} \times \mathcal{C}_\Omega \times SV_0(\Omega)$ for some given K_1, K_2 (see section 2 for details), namely, $\inf_{(\mathbf{u},m,s)\in\mathcal{A}\times\mathcal{C}_\Omega\times SV_0(\Omega)} S_{lc}(\mathbf{u}, m, s)$. This is a so-called "greedy problem" for joint diffeomorphic image registration and intensity correction, which searches for the global minimizer of the similarity $S_{lc}(\mathbf{u}, m, s)$ by placing the regularization into the constraint set $\mathcal{A} \times \mathcal{C}_\Omega \times SV_0(\Omega)$. The main contributions of the proposed multiscale approach contain three aspects:

- Propose a novel model for joint image registration and intensity correction.
- Address the greedy problem for joint image registration and intensity correction.
- Eliminate the intensity inhomogeneity by removing the bias.

The rest of this paper is organized as follows. In section 2, we propose a multiscale approach for (1.3) to address the "greedy problem." In section 3, an alternating direction method (ADM) method to solve the joint model for each scale is discussed and the convergence is also proved under some suitable assumptions. In section 4, we propose a coarse-to-fine strategy for the multiscale approach to further accelerate the algorithm. In section 5, some applications of the proposed multiscale approach are performed. Finally, we conclude our work and outline some problems for the future research in section 7.

2. Multiscale approach based on the model (1.3) and related greedy problem. Mesh folding may occur in the large deformation registration. To control the mesh folding in the large deformation registration, one can decompose the large deformation $\tilde{\boldsymbol{\varphi}}_n$ into the composition of some small deformations $\boldsymbol{\varphi}_i (i = 0, 1, 2, \ldots, n)$ [8, 20, 21], where $\boldsymbol{\varphi}_i$ is the deformation induced by different scales (different variational problems). This is where the "multiscale" comes from. Furthermore, we have two choices for this decomposition: (i) minimizing the functional that contains fidelity and regularization by keeping parameters unchanged for different scales [8] and (ii) minimizing the fidelity by setting some specific varying parameters for different scales [20, 21]. Motivated by [20, 21], we propose a multiscale approach based on the model (1.3) to give an answer to the question of whether or not one can find the global minimizer of $S_{lc}(\mathbf{u}, m, s)$ on $\mathcal{L}(\Omega) = \mathcal{A}(\Omega) \times \mathcal{C}_\Omega \times SV_0(\Omega)$. The multiscale approach is divided into the following n steps.

Step 0. Searching for the solution of the following variational problem:

$$(\mathbf{u}_0, m_0, s_0) \in \underset{(\mathbf{u},m,s)\in\mathcal{L}_{\varepsilon_0}(\Omega)}{\arg\min} J_0(\mathbf{u}, m, s), \tag{2.1}$$

where $J_0(\mathbf{u}, m, s) = \lambda_0 \int_\Omega (m(\mathbf{x}) + \ln D(\mathbf{x}) - \ln(T(\mathbf{x} + \mathbf{u}(\mathbf{x})) - s(\mathbf{x})))^2 d\mathbf{x} + \mu R(\mathbf{u}, m, s)$, $\mathcal{L}_{\varepsilon_0}(\Omega) = (\mathcal{A}(\Omega) \backslash \mathcal{B}_{\varepsilon_0}(\Omega)) \times \mathcal{C}_\Omega \times SV_0(\Omega)$, and $\varepsilon_0 > 0$. Define $\tilde{\boldsymbol{\varphi}}_0(\mathbf{x}) = \boldsymbol{\varphi}_0(\mathbf{x}) = \mathbf{x} + \mathbf{u}_0(\mathbf{x})$.

Step 1. Searching for the solution of the following variational problem:

$$(\mathbf{u}_1, \delta m_1, \delta s_1) \in \underset{(\mathbf{u},m_0+m,s_0+s)\in\mathcal{L}_{\varepsilon_1}(\Omega)}{\arg\min} J_1(\mathbf{u}, m, s),$$

where $J_1(\mathbf{u}, m, s) = \lambda_1 \int_\Omega (m_0(\mathbf{x}) + m(\mathbf{x}) + \ln D(\mathbf{x}) - \ln(T \circ \tilde{\boldsymbol{\varphi}}_0(\mathbf{x} + \mathbf{u}(\mathbf{x})) - s_0(\mathbf{x}) - s(\mathbf{x})))^2 d\mathbf{x} + \mu R(\mathbf{u}, m, s)$, $\mathcal{L}_{\varepsilon_1}(\Omega) = (\mathcal{A}(\Omega) \setminus \mathcal{B}_{\varepsilon_1}(\Omega)) \times \mathcal{C}_\Omega \times SV_0(\Omega)$, and $\varepsilon_1 > 0$. Define $\boldsymbol{\varphi}_1(\mathbf{x}) = \mathbf{x} + \mathbf{u}_1(\mathbf{x})$, $\tilde{\boldsymbol{\varphi}}_1(\mathbf{x}) = \tilde{\boldsymbol{\varphi}}_0 \circ \boldsymbol{\varphi}_1(\mathbf{x})$, $m_1(\mathbf{x}) = m_0(\mathbf{x}) + \delta m_1(\mathbf{x})$, and $s_1(\mathbf{x}) = s_0(\mathbf{x}) + \delta s_1(\mathbf{x})$.

$$\vdots$$

Step n. By induction, for $n \geq 1$, search for the solution of the following variational problem:

$$(\mathbf{u}_n, \delta m_n, \delta s_n) \in \underset{(\mathbf{u},m_{n-1}+m,s_{n-1}+s)\in\mathcal{L}_{\varepsilon_n}(\Omega)}{\arg\min} J_n(\mathbf{u}, m, s), \tag{2.2}$$

where $J_n(\mathbf{u}, m, s) = \lambda_n \int_\Omega (m_{n-1}(\mathbf{x}) + m(\mathbf{x}) + \ln D(\mathbf{x}) - \ln(T \circ \tilde{\boldsymbol{\varphi}}_{n-1}(\mathbf{x} + \mathbf{u}(\mathbf{x})) - s_{n-1}(\mathbf{x}) - s(\mathbf{x})))^2 d\mathbf{x} + \mu R(\mathbf{u}, m, s)$, $\mathcal{L}_{\varepsilon_n}(\Omega) = (\mathcal{A}(\Omega) \setminus \mathcal{B}_{\varepsilon_n}(\Omega)) \times \mathcal{C}_\Omega \times SV_0(\Omega)$, and $\varepsilon_n > 0$. Define $\boldsymbol{\varphi}_n(\mathbf{x}) = \mathbf{x} + \mathbf{u}_n(\mathbf{x})$, $\tilde{\boldsymbol{\varphi}}_n(\mathbf{x}) = \tilde{\boldsymbol{\varphi}}_{n-1} \circ \boldsymbol{\varphi}_n(\mathbf{x})$, $m_n(\mathbf{x}) = m_{n-1}(\mathbf{x}) + \delta m_n(\mathbf{x})$, and $s_n(\mathbf{x}) = s_{n-1}(\mathbf{x}) + \delta s_n(\mathbf{x})$.

Note that here the final deformation is $\tilde{\boldsymbol{\varphi}}_n(\mathbf{x}) = \boldsymbol{\varphi}_0 \circ \boldsymbol{\varphi}_1 \circ \cdots \circ \boldsymbol{\varphi}_n(\mathbf{x})$. This implies, when n is large enough (in practice, $n = 5$ is usually enough to achieve a convergent result), the multiscale approach (2.1)–(2.2) can simulate a large deformation well even if $\boldsymbol{\varphi}_i (i = 0, 1, \ldots, n)$ is a small deformation. In addition, there are two key parameters λ_n, ε_n in the multiscale approach (2.1)–(2.2). These parameters determine whether or not one can find the global minimizer of $S_{lc}(\mathbf{u}, m, s)$ on $\mathcal{L}(\Omega)$. In practice, λ_n and ε_n are set to be large numbers and small positive numbers, respectively. However, this is not enough. For example, similar to the idea in [8], by keeping λ_n as a large constant, one can only achieve the minimizer of $J(\mathbf{u}, m, s)$. In addition, the ratio λ_n of fidelity may change with scale number n. That is, the final deformation is the composition of the deformations of different variational problems. This is the outcome where the multiscale comes from.

In order to use the multiscale approach (2.1)–(2.2) to solve the greedy matching problem well, we shall give a more precise condition shortly (i.e., λ_n and ϵ_n satisfy the convergence condition in Theorem 2.6).

Before that, concerning the existence of the solution for (2.2), we have the following result.

THEOREM 2.1. *Assume that* $\max_{\mathbf{x}\in\Omega}|T(\mathbf{x})| < M < +\infty$, $\max_{\mathbf{x}\in\Omega}|D(\mathbf{x})| < M < +\infty$, *and* $\triangle_T \triangleq \{\mathbf{x} : T(\mathbf{x})$ is discontinuous at $\mathbf{x}\}$ *is a zero measure set; then there exists at least one solution for* (2.2).

Proof. By selecting a minimizing sequence $\{(\mathbf{u}^k, \delta m^k, \delta s^k)\}$ of the functional $J_n(\mathbf{u}, \delta m, \delta s)$, due to $J_n(\mathbf{u}, \delta m, \delta s) \le J_n(\mathbf{0}, 0, 0)$, one can conclude that $\mathbf{u}^k$, δm^k, and δs^k are bounded on $[H^\alpha(\Omega)]^2$, $BV_0(\Omega)$, and $BV_0(\Omega)$, respectively.

Firstly, by the compactness of $H^\alpha(\Omega)$, there exists a subsequence of $\mathbf{u}^k$ which is still labeled by k and $\mathbf{u} \in [H^\alpha(\Omega)]^2$ such that $\mathbf{u}^k$ weakly converges to $\mathbf{u}$ with $R_1(\mathbf{u}) \le \lim_{k\to\infty} \inf R_1(\mathbf{u}^k)$. By the compact embedding theorem (Theorem 4.58 in [9]), we know that $H_0^\alpha(\Omega) \hookrightarrow C^1(\Omega)$. Namely, there exists a subsequence of $\mathbf{u}^k$ which is still labeled by k and $\bar{\mathbf{u}} \in [C^1(\Omega)]^2$ such that $\mathbf{u}^k$ converges to $\bar{\mathbf{u}}$ in $[C^1(\Omega)]^2$. Moreover, by the uniqueness of the limit, we get $\bar{\mathbf{u}} = \mathbf{u}$. That is, $\mathbf{u}^k \xrightarrow{k} \mathbf{u}$ in $[C^1(\Omega)]^2$. Therefore, we conclude $\mathbf{u} \in \mathcal{A}(\Omega) \setminus \mathcal{B}_{\varepsilon_n}(\Omega)$.

Secondly, by the compactness on $BV(\Omega)$, there exists a subsequence of δm^k which is still labeled by k and $\delta m \in BV(\Omega)$ such that δm^k weakly converges to δm with

$$\|\delta m^k - \delta m\|_{L^1(\Omega)} \xrightarrow{k} 0 \text{ and } \int_\Omega \nabla \delta m^k \cdot \varphi d\mathbf{x} \xrightarrow{k} \int_\Omega \nabla \delta m \cdot \varphi d\mathbf{x} \quad \forall \varphi \in C_0^\infty(\Omega), \tag{2.3}$$

where the first equation in (2.3) implies $m_{n-1} + \delta m \in C_\Omega$, and the second equation in (2.3) implies $R_2(m^k) \xrightarrow{k} R_2(m)$.

Similarly to the analysis on δm^k, one can again conclude that there exists a subsequence of δs^k which is still labeled by k and $\delta s \in BV(\Omega)$ such that δs^k weakly converges to δs with

$$\|\delta s^k - \delta s\|_{L^1(\Omega)} \xrightarrow{k} 0 \text{ and } \int_\Omega \nabla \delta s^k \cdot \varphi d\mathbf{x} \xrightarrow{k} \int_\Omega \nabla \delta s \cdot \varphi d\mathbf{x} \quad \forall \varphi \in C_0^\infty(\Omega), \tag{2.4}$$

where the first equation in (2.4) implies $s_{n-1} + \delta m \in SV_0(\Omega)$, and the second equation in (2.4) implies $R_3(\delta s^k) \xrightarrow{k} R_3(\delta s)$.

Finally, by $\|\mathbf{u}^k - \mathbf{u}\|_{[C^1(\Omega)]^2} \xrightarrow{k} 0$, $\|\delta m^k - \delta m\|_{L^1(\Omega)} \xrightarrow{k} 0$ and $\|\delta s^k - \delta s\|_{L^1(\Omega)} \xrightarrow{k} 0$, we obtain $\int_\Omega (m_{n-1}(\mathbf{x}) + \delta m^k(\mathbf{x}) + \ln D(\mathbf{x}) - \ln(T \circ \tilde{\boldsymbol{\varphi}}_{n-1}(\mathbf{x} + \mathbf{u}^k(\mathbf{x})) - s_{n-1}(\mathbf{x}) - \delta s^k(\mathbf{x})))^2 d\mathbf{x} \xrightarrow{k} \int_\Omega (m_{n-1}(\mathbf{x}) + \delta m(\mathbf{x}) + \ln D(\mathbf{x}) - \ln(T \circ \tilde{\boldsymbol{\varphi}}_{n-1}(\mathbf{x} + \mathbf{u}(\mathbf{x})) - s_{n-1}(\mathbf{x}) - \delta s(\mathbf{x})))^2 d\mathbf{x}$. Note that here we use $\tilde{\boldsymbol{\varphi}}_{n-1} \in [C^1(\Omega)]^2$, which implies that $T \circ \tilde{\boldsymbol{\varphi}}_{n-1}(\cdot)$ is continuous except on some zero measure set. Therefore, $J_n(\mathbf{u}, \delta m, \delta s) \le \lim_{k\to\infty} \inf J_n(\mathbf{u}^k, \delta m^k, \delta s^k)$, which ensures the existence of solution for (2.2). ∎

Then recall some important lemmas in [20], which are necessary for the proof of the convergence of the multiscale approach (2.1)–(2.2).

LEMMA 2.2. *Assume* $\mathbf{f}, \mathbf{g} : \Omega \to \Omega$, $\mathcal{W}(\mathbf{f}) = \mathbf{f} - \mathbf{I}$, *and* $\mathbf{I}$ *is the identity mapping; then there holds the following:*

(i) *If* $\mathcal{W}(\mathbf{f}) \in \mathcal{A}(\Omega) \setminus \mathcal{B}_{\varepsilon_1}(\Omega)$, $\mathcal{W}(\mathbf{g}) \in \mathcal{A}(\Omega) \setminus \mathcal{B}_{\varepsilon_2}(\Omega)$, *then* $\mathcal{W}(\mathbf{f} \circ \mathbf{g}) \in \mathcal{A}(\Omega) \setminus \mathcal{B}_{\varepsilon_1\varepsilon_2}(\Omega)$.

(ii) *If* $\mathcal{W}(\mathbf{f}) \in \mathcal{A}(\Omega) \setminus \mathcal{B}_\varepsilon(\Omega)$, *then there exists* $\mathbf{g} = \mathbf{f}^{-1} \in \mathcal{A}(\Omega)$.

(iii) *If* $\mathcal{W}(\mathbf{g}) \in \mathcal{A}(\Omega) \setminus \mathcal{B}_\varepsilon(\Omega)$, *then there exists a constant* C_1 *such that* $\int_\Omega \mathbf{f}(\mathbf{g}(\mathbf{x}))d\mathbf{x} \le C_1 R_1(\mathbf{g}^{-1}) \int_\Omega \mathbf{f}(\mathbf{y})d\mathbf{y}$.

Remark 2.3. Recall that the deformation $\boldsymbol{\varphi} : \Omega \to \Omega$ is defined to be the sum of the identity map and displacement $\mathbf{u} : \Omega \to \mathbb{R}$, namely, $\boldsymbol{\varphi}(\mathbf{x}) = \mathbf{x} + \mathbf{u}(\mathbf{x})$. Here, the operator $\mathcal{W}$ is introduced to distinguish the deformation and displacement and simplify the description in the proof of Theorem 2.6. In fact, $\mathcal{W}(\boldsymbol{\varphi}) = \mathbf{u}$.

LEMMA 2.4. *Assume* $\mathbf{p}(\mathbf{x}) = \mathbf{x} + \mathbf{u}(\mathbf{x})$ *and* $\mathcal{W}(\mathbf{q}) \in \mathcal{A}(\Omega) \setminus \mathcal{B}_\varepsilon(\Omega)$*; then there exists a constant* C_2 *such that* $R_1(\mathcal{W}(\mathbf{p} \circ \mathbf{q})) = 2(R_1(\mathcal{W}(\mathbf{q})) + C_2 R_1(\mathbf{q}^{-1}) R_1(\mathcal{W}(\mathbf{p})))$.

LEMMA 2.5. *Assume* $\boldsymbol{\varphi}(\mathbf{x}) = \mathbf{x} + \mathbf{u}(\mathbf{x})$, $\mathbf{g}(\mathbf{x}) = \boldsymbol{\varphi}^{-1}(\mathbf{x}) = \mathbf{x} + \mathbf{v}(\mathbf{x})$, *and* $\mathbf{u}, \mathbf{v} \in \mathcal{A}(\Omega) \setminus \mathcal{B}_\varepsilon(\Omega)$*; then there exists a constant* C_3 *such that* $R_1(\mathbf{u}) = \int_\Omega \|\nabla^\alpha \mathbf{u}(\mathbf{x})\|^2 d\mathbf{x} \le C_3 R_1(\mathbf{g}) R_1(\mathcal{W}(\mathbf{g}))$.

Based on these lemmas, we are now ready to give the result on the convergence of the multiscale approach (2.1)–(2.2).

By setting $m \equiv 0$, $s \equiv 0$, and $\mathbf{u} \equiv \mathbf{0}$, it follows from $J_n(\mathbf{u}_n, \delta m_n, \delta s_n) \le J_n(\mathbf{0}, 0, 0)$ in (2.2) that

$$\lambda_n S_{lc}^n(\mathbf{u}_n, m_n, s_n) + \mu R(\mathbf{u}_n, \delta m_n, \delta s_n) \le \lambda_n S_{lc}^{n-1}(\mathbf{u}_{n-1}, m_{n-1}, s_{n-1}),$$

where

$$S_{lc}^n(\mathbf{u}_n, m_n, s_n) = \int_\Omega (m_n(\mathbf{x}) + \ln D(\mathbf{x}) - \ln(T \circ \tilde{\boldsymbol{\varphi}}_n(\mathbf{x}) - s_n(\mathbf{x})))^2 d\mathbf{x},$$

and $R(\mathbf{0}, 0, 0) = 0$. Hence, $S_{lc}^n(\mathbf{u}_n, m_n, s_n)$ is a decreasing sequence with a lower bound, whose limit is defined by

$$\delta = \lim_{n \to +\infty} S_{lc}^n(\mathbf{u}_n, m_n, s_n). \tag{2.5}$$

Define

$$\phi = \inf_{(\mathbf{u}, m, s) \in \mathcal{L}(\Omega)} \int_\Omega (m(\mathbf{x}) + \ln D(\mathbf{x}) - \ln(T(\mathbf{x} + \mathbf{u}(\mathbf{x})) - s(\mathbf{x})))^2 d\mathbf{x}. \tag{2.6}$$

By proving $\delta = \phi$ under some suitable assumptions, we can give an answer to the problem of whether or not one can find the global minimizer of $S_{lc}(\mathbf{u}, m, s)$ on a proper set $\mathcal{L}(\Omega) = \mathcal{A}(\Omega) \times \mathcal{C}_\Omega \times SV_0(\Omega)$. Note that (1.4)–(1.6) imply $\mathcal{A}(\Omega) \subseteq [H_0^\alpha(\Omega)]^2$, $\mathcal{C}_\Omega \subseteq BV(\Omega)$, and $SV_0(\Omega) \subseteq BV(\Omega)$, which ensures that the greedy matching problem (2.6) is well regularized.

THEOREM 2.6. *Let* $\boldsymbol{\varphi}_n$, $\tilde{\boldsymbol{\varphi}}_n$, m_n, *and* s_n *be induced by the multiscale approach* (2.1)–(2.2)*, and assume that* B, M, *and* λ_n *are three positive numbers satisfying* $\lim_{n \to +\infty} \frac{B^{4n-3} M^{4^n}}{\lambda_n} = 0$ *and* $\lim_{n \to +\infty} \varepsilon_n = 0$*, where* B *is a positive number depending on* Ω *and* M *is a positive number depending on* $\mathbf{u}_0$, δm_0, δs_0, Ω, α, *and* ϕ*, respectively. Then there holds* $\phi = \delta$.

Proof. It is obvious that $\delta \ge \phi$. To show $\delta \le \phi$, we use the contradiction.

Assume $\delta > \phi$; then there exists a $C_1 \in (0, 1)$ such that $\phi < C_1 \delta < \delta$. By the definition of ϕ, there exists $\bar{\boldsymbol{\varphi}}(\mathbf{x}) = \mathbf{x} + \bar{\mathbf{u}}(\mathbf{x}) \in \mathcal{A}(\Omega)$, $\bar{m} \in \mathcal{C}_\Omega$, and $\bar{s} \in SV_0(\Omega)$ such that

$$\|\bar{m} + \ln D - \ln(T \circ \bar{\boldsymbol{\varphi}} - \bar{s})\|_{L^2(\Omega)}^2 < C_1 \delta. \tag{2.7}$$

Setting $\boldsymbol{\varphi} = \tilde{\boldsymbol{\varphi}}_{n-1}^{-1} \circ \bar{\boldsymbol{\varphi}}$, $m = \bar{m} - m_{n-1}$, $s = \bar{s} - s_{n-1}$, by Lemma 2.2, we obtain $\boldsymbol{\varphi} \in \mathcal{A}(\Omega)$, $m_{n-1} + m \in \mathcal{C}_\Omega$, and $s_{n-1} + s \in SV_0(\Omega)$. By (2.2), (2.5), and (2.7), we have

(2.8)
$$\begin{aligned}\lambda_n \int_\Omega (\tilde{m}_n(\mathbf{x}) + \ln D(\mathbf{x}) - \ln(T\circ\tilde{\boldsymbol{\varphi}}_n(\mathbf{x}) - \tilde{s}_n(\mathbf{x})))^2 d\mathbf{x} + \mu R(\mathbf{u}_n, \delta m_n, \delta s_n)\\ \le \lambda_n \|\bar{m} + \ln D - \ln(T\circ\boldsymbol{\varphi} - \bar{s})\|^2_{L^2(\Omega)} + \mu R(\mathcal{W}(\tilde{\boldsymbol{\varphi}}_{n-1}^{-1}\circ\bar{\boldsymbol{\varphi}}), \bar{m} - m_{n-1}, \bar{s} - s_{n-1})\\ \le \lambda_n C_1 \delta + \mu R(\mathcal{W}(\tilde{\boldsymbol{\varphi}}_{n-1}^{-1}\circ\bar{\boldsymbol{\varphi}}), \bar{m} - m_{n-1}, \bar{s} - s_{n-1}).\end{aligned}$$

Then by (2.8), we further have

$$\lambda_n(1 - C_1)\delta + \mu R(\mathbf{u}_n, \delta m_n, \delta s_n) \le \mu R(\mathcal{W}(\tilde{\boldsymbol{\varphi}}_{n-1}^{-1}\circ\bar{\boldsymbol{\varphi}}), \bar{m} - m_{n-1}, \bar{s} - s_{n-1}) \tag{2.9}$$

and

$$R(\mathbf{u}_n, \delta m_n, \delta s_n) \le R(\mathcal{W}(\tilde{\boldsymbol{\varphi}}_{n-1}^{-1}\circ\bar{\boldsymbol{\varphi}}), \bar{m} - m_{n-1}, \bar{s} - s_{n-1}). \tag{2.10}$$

Recall $R(\mathbf{u}, m, s) = R_1(\mathbf{u}) + R_2(m) + R_3(s)$. Based on the inequality $|a + b| \le |a| + |b|$ and the fact $m_{n-1} = m_{n-2} + \delta m_{n-1}$, $s_{n-1} = s_{n-2} + \delta s_{n-1}$, we obtain

$$\begin{aligned}&R_2(\bar{m} - m_{n-1}) \le R_2(\bar{m} - m_{n-2}) + R_2(\delta m_{n-1}),\ R_3(\bar{s} - s_{n-1}) \le R_3(\bar{s} - s_{n-2})\\ &\quad + R_3(\delta s_{n-1}).\end{aligned} \tag{2.11}$$

To estimate $R_1(\mathcal{W}(\tilde{\boldsymbol{\varphi}}_{n-1}^{-1}\circ\bar{\boldsymbol{\varphi}}))$, by Lemma 2.4, we obtain

(2.12)
$$R_1(\mathcal{W}(\tilde{\boldsymbol{\varphi}}_{n-1}^{-1}\circ\bar{\boldsymbol{\varphi}})) \le 2R_1(\mathcal{W}(\tilde{\boldsymbol{\varphi}}_{n-2}^{-1}\circ\bar{\boldsymbol{\varphi}})) + 2CR_1((\tilde{\boldsymbol{\varphi}}_{n-2}^{-1}\circ\bar{\boldsymbol{\varphi}})^{-1})R_1(\mathcal{W}(\boldsymbol{\varphi}_{n-1}^{-1})),$$

where we use the formula $\tilde{\boldsymbol{\varphi}}_{n-1}^{-1}\circ\bar{\boldsymbol{\varphi}} = \boldsymbol{\varphi}_{n-1}^{-1}\circ\tilde{\boldsymbol{\varphi}}_{n-2}^{-1}\circ\bar{\boldsymbol{\varphi}} = \boldsymbol{\varphi}_{n-1}^{-1}\circ(\tilde{\boldsymbol{\varphi}}_{n-2}^{-1}\circ\bar{\boldsymbol{\varphi}})$. Concerning the estimates on $R_1((\tilde{\boldsymbol{\varphi}}_{n-2}^{-1}\circ\bar{\boldsymbol{\varphi}})^{-1})$ and $R_1(\mathcal{W}(\boldsymbol{\varphi}_{n-1}^{-1}))$, we have

$$\begin{aligned}R_1((\tilde{\boldsymbol{\varphi}}_{n-2}^{-1}\circ\bar{\boldsymbol{\varphi}})^{-1}) &\le 2R_1(\mathbf{x}) + 2R_1(\mathcal{W}((\tilde{\boldsymbol{\varphi}}_{n-2}^{-1}\circ\bar{\boldsymbol{\varphi}})^{-1}))\\ &\le \tilde{c}_1 R_1(\tilde{\boldsymbol{\varphi}}_{n-2}^{-1}\circ\bar{\boldsymbol{\varphi}})R_1(\mathcal{W}((\tilde{\boldsymbol{\varphi}}_{n-2}^{-1}\circ\bar{\boldsymbol{\varphi}}))) + \tilde{c}_2\\ &\le \tilde{c}_3 R_1^2(\mathcal{W}(\tilde{\boldsymbol{\varphi}}_{n-2}^{-1}\circ\bar{\boldsymbol{\varphi}})) + \tilde{c}_4 R_1(\mathcal{W}(\tilde{\boldsymbol{\varphi}}_{n-2}^{-1}\circ\bar{\boldsymbol{\varphi}})) + \tilde{c}_5\\ &\le B_1\mathcal{M}^2((R_1(\mathcal{W}(\tilde{\boldsymbol{\varphi}}_{n-2}^{-1}\circ\bar{\boldsymbol{\varphi}}))))\end{aligned} \tag{2.13}$$

and

$$\begin{aligned}R_1(\mathcal{W}(\boldsymbol{\varphi}_{n-1}^{-1})) &\le CR_1(\mathcal{W}(\boldsymbol{\varphi}_{n-1}))R_1(\boldsymbol{\varphi}_{n-1})\\ &\le CR_1(\mathcal{W}(\boldsymbol{\varphi}_{n-1}))(\bar{C} + R_1(\mathcal{W}(\boldsymbol{\varphi}_{n-1})))\\ &\le B_0\mathcal{M}^2(R_1(\mathcal{W}(\boldsymbol{\varphi}_{n-1}))),\end{aligned} \tag{2.14}$$

where, for any $\xi \ge 0$,

$$\mathcal{M}(\xi) = \begin{cases} 1, & 0 \le \xi \le 1,\\ \xi, & \xi > 1.\end{cases}$$

The first and third inequalities in (2.13) are based on the fact that $\mathbf{f}(\mathbf{x}) = \mathbf{x} + \mathcal{W}(\mathbf{f})$ for any deformation $\mathbf{f}$, and the second inequality in (2.13) is based on the conclusion $R_1(\mathcal{W}(\mathbf{g}^{-1})) \le CR_1(\mathbf{g})R_1(\mathcal{W}(\mathbf{g}))$ in Lemma 2.5. Hence, by (2.12), (2.13), and (2.14), we get

$$\begin{aligned}R_1(\mathcal{W}(\tilde{\boldsymbol{\varphi}}_{n-1}^{-1}\circ\bar{\boldsymbol{\varphi}})) \le{}& 2R_1(\mathcal{W}(\tilde{\boldsymbol{\varphi}}_{n-2}^{-1}\circ\bar{\boldsymbol{\varphi}}))\\ &+ B\mathcal{M}^2(R_1(\mathcal{W}(\boldsymbol{\varphi}_{n-1})))\mathcal{M}^2(R_1(\mathcal{W}(\tilde{\boldsymbol{\varphi}}_{n-2}^{-1}\circ\bar{\boldsymbol{\varphi}}))).\end{aligned} \tag{2.15}$$

Furthermore, by (2.10), (2.11), and (2.15), we have

$$
\begin{aligned}
&R(\mathcal{W}(\tilde{\boldsymbol{\varphi}}_{n-1}^{-1}\circ\bar{\boldsymbol{\varphi}}),\bar{m}-m_{n-1},\bar{s}-s_{n-1})\\
&\quad\le 2R(\mathcal{W}(\tilde{\boldsymbol{\varphi}}_{n-2}^{-1}\circ\bar{\boldsymbol{\varphi}}),\bar{m}-m_{n-2},\bar{s}-s_{n-2})+\bar{B}\mathcal{M}^4[R(\mathcal{W}(\tilde{\boldsymbol{\varphi}}_{n-2}^{-1}\circ\bar{\boldsymbol{\varphi}}),\\
&\qquad \bar{m}-m_{n-2},\bar{s}-s_{n-2})]\\
&\quad\le B\mathcal{M}^4[R(\mathcal{W}(\tilde{\boldsymbol{\varphi}}_{n-2}^{-1}\circ\bar{\boldsymbol{\varphi}}),\bar{m}-m_{n-2},\bar{s}-s_{n-2})]\\
&\quad\le\cdots\\
&\quad\le B^{4n-3}\mathcal{M}^{4^n}[R(\mathcal{W}(\tilde{\boldsymbol{\varphi}}_0^{-1}\circ\bar{\boldsymbol{\varphi}}),\bar{m}-m_0,\bar{s}-s_0)].
\end{aligned}
\tag{2.16}
$$

Define $M\triangleq\mathcal{M}[R(\mathcal{W}(\tilde{\boldsymbol{\varphi}}_0^{-1}\circ\bar{\boldsymbol{\varphi}}),\bar{m}-m_0,\bar{s}-s_0)]$. By (2.9) and (2.16), we then obtain $1-C_1\le 0$ as $n\to+\infty$, which contradicts $C_1\in(0,1)$. Therefore, $\delta=\phi$. ∎

Remark 2.7. By Theorem 2.6, the multiscale approach (2.1)–(2.2) provides a solution to the following "greedy problem":

$$
\inf_{(\mathbf{u},m,s)\in\mathcal{L}(\Omega)} S_{lc}(\mathbf{u},m,s). \tag{2.17}
$$

Here, a key point is that the regularization in (2.17) is reflected on $\mathcal{L}(\Omega)=\mathcal{A}(\Omega)\times\mathcal{C}_\Omega\times SV_0(\Omega)$. Otherwise, the trivial solution (i.e., $\mathbf{u}=\mathbf{0}$, $m=\frac{T}{D}$, $s=0$) may occur. In our method, some constraints (i.e., $\mathbf{u}\in\mathcal{A}(\Omega)$, $m\in\mathcal{C}_\Omega$, $s\in SV_0(\Omega)$) are additionally added in (1.4)–(1.6). Compared with the greedy problem in [20] that has nothing to do with parameters, the result of the greedy problem (2.17) is affected by two parameters K_1 and K_2, since the constraint $\mathcal{C}_\Omega$ is determined by parameters K_1 and K_2. In applications, a practitioner needs to give some estimates on the intensity of varying illumination and set suitable K_1,K_2 (i.e., K_1,K_2 are suggested to be set near zero if no varying illumination in image pairs); then the multiscale approach (2.1)–(2.2) can work well to produce some expected solutions.

3. ADM for (2.2). In this section, we mainly focus on the numerical implementation of the proposed multiscale approach (2.1)–(2.2) with λ_n and ε_n chosen by Theorem 2.6 (i.e., $\lambda_n=a^n\times b^{4^n}$ for some $a,b>1$ and $\varepsilon_n=\frac{\varepsilon_0}{2^n}$ for some $\varepsilon_0\in(0,1)$). To address the nonconvexity of $S_{lc}(\mathbf{u},m,s)$, an auxiliary variable $\mathbf{v}$ is additionally introduced and (2.2) is reformulated as follows:

$$
(\mathbf{v}_n,\mathbf{u}_n,\delta m_n,\delta s_n)\in\underset{(\mathbf{v},\mathbf{u},m_{n-1}+m,s_{n-1}+s)\in\overline{\mathcal{L}}_{\varepsilon_n}(\Omega)}{\arg\min} E_n(\mathbf{v},\mathbf{u},m,s), \tag{3.1}
$$

where

$$
\begin{aligned}
&E_n(\mathbf{v},\mathbf{u},m,s)\\
&\quad=\lambda_n\int_\Omega(m_{n-1}(\mathbf{x})+m(\mathbf{x})+\ln D(\mathbf{x})-\ln(T\circ\tilde{\boldsymbol{\varphi}}_{n-1}(\mathbf{x}+\mathbf{v}(\mathbf{x}))-s_{n-1}(\mathbf{x})-s(\mathbf{x})))^2d\mathbf{x}\\
&\qquad+\mu R(\mathbf{u},m,s)+\Theta R_c(\mathbf{u})+\frac{1}{2\theta_n}\int_\Omega|\mathbf{v}-\mathbf{u}|^2d\mathbf{x},
\end{aligned}
$$

$R_c(\mathbf{u})=\int_\Omega(\frac{\partial u_1}{\partial x_1}-\frac{\partial u_2}{\partial x_2})^2+(\frac{\partial u_1}{\partial x_2}+\frac{\partial u_2}{\partial x_1})^2d\mathbf{x}$, $\overline{\mathcal{L}}_{\varepsilon_n}(\Omega)=L^2(\Omega)\times\mathcal{L}_{\varepsilon_n}(\Omega)$, $\theta_n>0$ is a small number, and $\Theta>0$ is a large number.

Remark 3.1. Here the penalty term $R_c(\mathbf{u})$ comes from [18] to relax the conformal constraint. In fact, $R_c(\mathbf{u})=0$ when $\boldsymbol{\varphi}(\mathbf{x})=\mathbf{x}+\mathbf{u}(\mathbf{x})$ is in conformal set. Therefore, $R_c(\mathbf{u})=\int_\Omega(\frac{\partial u_1}{\partial x_1}-\frac{\partial u_2}{\partial x_2})^2+(\frac{\partial u_1}{\partial x_2}+\frac{\partial u_2}{\partial x_1})^2d\mathbf{x}$ can be viewed as the distance between the

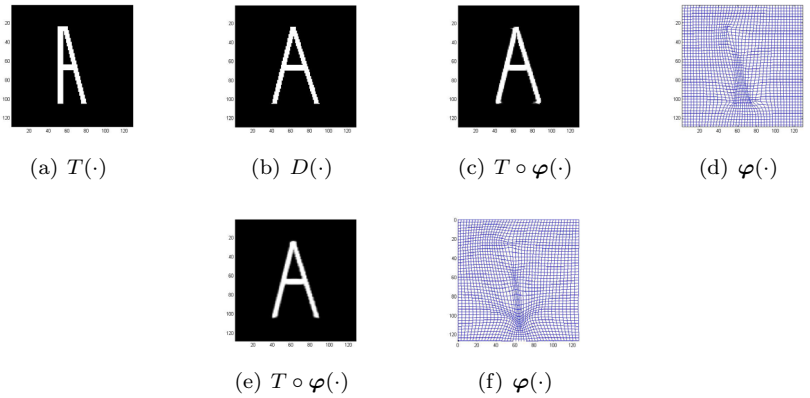

(a) $T(\cdot)$ (b) $D(\cdot)$ (c) $T \circ \boldsymbol{\varphi}(\cdot)$ (d) $\boldsymbol{\varphi}(\cdot)$

(e) $T \circ \boldsymbol{\varphi}(\cdot)$ (f) $\boldsymbol{\varphi}(\cdot)$

FIG. 3. *Comparison between the relaxed Cauchy–Riemann model* [18] *and the quasi-conformal model* [40]*:* (a) *and* (b) *are floating image and target image, respectively;* (c) *and* (d) *are registration results of the relaxed Cauchy–Riemann model* [18] *with* Re_SSD $= 3.21\%$*;* (e) *and* (f) *are registration results of the quasi-conformal model* [40] *with* Re_SSD $= 4.63\%$.

mapping $\boldsymbol{\varphi}$ and conformal set. In this view, by setting some approximate regularization, the relaxed model (2.1) in [18] is equivalent to the quasi-conformal model in [40] which also minimizes the distance

$$\int_{\Omega} \frac{\|\nabla \boldsymbol{\varphi}(\mathbf{x})\|_F^2}{2 \det(\nabla \boldsymbol{\varphi}(\mathbf{x}))} d\mathbf{x} \tag{3.2}$$

between mapping $\boldsymbol{\varphi}$ and conformal set in some sense. To illustrate this idea, the comparison results for these two models are listed on Figure 3. In this comparison, one can note that the relaxed model [18] and the quasi-conformal model [40] achieve the same type of deformation. Besides, the distance defined in (3.2) has the ability to control the minimal value of $\det(\nabla \boldsymbol{\varphi})$ (because $\det(\nabla \boldsymbol{\varphi})$ acts as the denominator of the objective functional) while the distance $R_c(\mathbf{u})$ does not work on this aspect. That is, $R_c(\mathbf{u})$ controls less than (3.2). This is the reason why the relaxed model [18] achieves a lower quality (smaller $\min_{\mathbf{x}\in\Omega} \det(\nabla \boldsymbol{\varphi}(\mathbf{x}))$) deformation but smaller Re_SSD. Moreover, the relaxed model also works for the landmark registration by deleting the fidelity term of the relaxed model [18] (Figure 4). Based on these comparisons and to make further analysis much easier, we use the relaxed conformal constraint $R_c(\mathbf{u})$ (with much simpler structure) to control the mesh folding in this paper.

Then setting an initialization $\mathbf{v}_n^0 = \mathbf{0}$, $\mathbf{u}_n^0 = \mathbf{0}$, $\delta m_n^0 = 0$, $\delta s_n^0 = 0$ for some given scale n, (3.1) can be split into the following four subproblems:

$$\mathbf{v}_n^{k+1} \in \underset{\mathbf{v}\in[L^2(\Omega)]^2}{\arg\min} \; E_n(\mathbf{v}, \mathbf{u}_n^k, \delta m_n^k, \delta s_n^k), \tag{3.3}$$

$$\mathbf{u}_n^{k+1} \in \underset{\mathbf{u}\in[H_0^\alpha(\Omega)]^2}{\arg\min} \; E_n(\mathbf{v}_n^{k+1}, \mathbf{u}, \delta m_n^k, \delta s_n^k), \tag{3.4}$$

$$\delta m_n^{k+1} = \underset{m_{n-1}+m\in\mathcal{C}_\Omega}{\arg\min} \; E_n(\mathbf{v}_n^{k+1}, \mathbf{u}_n^{k+1}, m, \delta s_n^k), \tag{3.5}$$

$$\delta s_n^{k+1} = \underset{s_{n-1}+s\in SV_0(\Omega)}{\arg\min} \; E_n(\mathbf{v}_n^{k+1}, \mathbf{u}_n^{k+1}, \delta m_n^{k+1}, s), \tag{3.6}$$

for $k = 0, 1, 2, \ldots$.

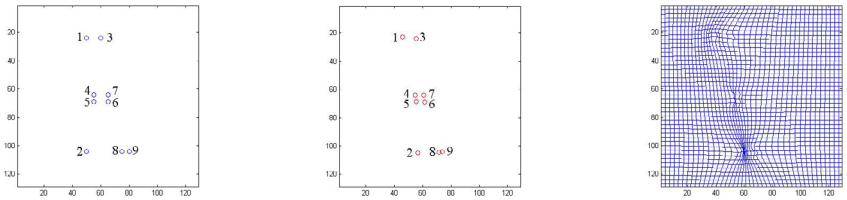

(a) (b) (c)

FIG. 4. *Landmark registration by the relaxed Cauchy–Riemann model* [18]*:* (a) *and* (b) *are the labels for the floating image and target image* ($\boldsymbol{\varphi}(\mathbf{x}_i) = \mathbf{y}_i (i = 1, 2, \ldots, 9)$*, respectively;* (c) *is the deformation induced by deleting the fidelity term of the relaxed Cauchy–Riemann model* [18].

Concerning the convergence of $\{(\mathbf{v}_n^k, \mathbf{u}_n^k, \delta m_n^k, \delta s_n^k)\}$, here, we assume $\alpha > 3$ for the technical demand to ensure $\boldsymbol{\varphi} \in [C^2(\Omega)]^2$ ($H_0^\alpha(\Omega) \hookrightarrow C^2(\Omega)$ ($\alpha > 3$) (see Theorem 4.58 in [9]). Before showing the convergence result, we give some lemmas for subproblems (3.3)–(3.6), which will be used in the later proof.

LEMMA 3.2. *Suppose* $\alpha > 3$, $T(\cdot)$ *is twice differentiable with* $\operatorname{ess\,sup}_{\mathbf{x}\in\Omega} |T(\mathbf{x})| < \bar{M} < +\infty$, $\operatorname{ess\,sup}_{\mathbf{x}\in\Omega} |D(\mathbf{x})| < \bar{M} < +\infty$, $0 < \theta_n < \frac{(\kappa-\kappa_0)^2}{10\overline{M}^2(\lambda_n \widetilde{M})^n}$, $\operatorname{ess\,sup}_{\mathbf{x}\in\Omega} |\nabla T(\mathbf{x})| < \bar{M} < +\infty$, *and* $\operatorname{ess\,sup}_{\mathbf{x}\in\Omega} |\nabla^2 T(\mathbf{x})| < \bar{M} < +\infty$, *where* $\widetilde{M} \triangleq \widetilde{M}(\Omega, \alpha) = 2C|\Omega|[K^2 + \ln^2(\overline{M}/\kappa)^2] > 0$, $K = \max\{|K_1|, |K_2|\}$, *and* $C = C(\Omega, \alpha)$ *is a positive constant (see Lemma* 3.2 *and* 3.3 *in* [16] *for details). Then for the subproblem* (3.3)*, there exists a constant* $c > 0$ *such that*

(3.7)
$$-2\lambda_n(m_{n-1} + m_n^k + \ln D - \ln T_n^{k+1}) \frac{\nabla_{\mathbf{v}} T \circ \tilde{\boldsymbol{\varphi}}_{n-1}(\mathbf{x} + \mathbf{v}_n^{k+1})}{T_n^{k+1}} + \frac{1}{\theta_n}(\mathbf{v}_n^{k+1} - \mathbf{u}_n^k) = 0$$

and

$$E_n(\mathbf{v}_n^k, \mathbf{u}_n^k, \delta m_n^k, \delta s_n^k) - E_n(\mathbf{v}_n^{k+1}, \mathbf{u}_n^k, \delta m_n^k, \delta s_n^k) \geq c\|\mathbf{v}_n^{k+1} - \mathbf{v}_n^k\|^2_{[L^2(\Omega)]^2}.$$

Here and in what follows, $T_n^{k+1} = T \circ \tilde{\boldsymbol{\varphi}}_{n-1}(\mathbf{x} + \mathbf{v}_n^{k+1}) - s_{n-1} - \delta s_n^k$.

Proof. The first-order variation of (3.3) is

$$\begin{aligned} &-2\lambda_n \int_\Omega (m_{n-1} + m_n^k + \ln D - \ln T_n^{k+1}) \frac{\nabla_{\mathbf{v}} T \circ \tilde{\boldsymbol{\varphi}}_{n-1}(\mathbf{x} + \mathbf{v}_n^{k+1})}{T_n^{k+1}} \cdot \mathbf{z}(\mathbf{x}) d\mathbf{x} \\ &+ \frac{1}{\theta_n} \int_\Omega (\mathbf{v}_n^{k+1} - \mathbf{u}_n^k) \cdot \mathbf{z}(\mathbf{x}) d\mathbf{x} = 0, \end{aligned} \tag{3.8}$$

where $\mathbf{z}$ is the test function. By the variational principle, this concludes (3.7).

Letting $\mathbf{z} = \mathbf{v}_n^k - \mathbf{v}_n^{k+1}$ in (3.8), it yields

$$\begin{aligned} L(\mathbf{v}_n^k, \mathbf{v}_n^{k+1}) = \int_\Omega &(-2\lambda_n(m_{n-1} + \delta m_n^k + \ln D - \ln T_n^{k+1}) \frac{\nabla_{\mathbf{v}} T \circ \tilde{\boldsymbol{\varphi}}_{n-1}(\mathbf{x} + \mathbf{v}_n^{k+1})}{T_n^{k+1}} \\ &+ \frac{1}{\theta_n}(\mathbf{v}_n^{k+1} - \mathbf{u}_n^k)) \cdot (\mathbf{v}_n^k - \mathbf{v}_n^{k+1}) d\mathbf{x} = 0. \end{aligned}$$

Then we have

(3.9)
$$
\begin{aligned}
&E_n(\mathbf{v}_n^k,\mathbf{u}_n^k,\delta m_n^k,\delta s_n^k)-E_n(\mathbf{v}_n^{k+1},\mathbf{u}_n^k,\delta m_n^k,\delta s_n^k)\\
&=\lambda_n\int_\Omega \ln\frac{T\circ\tilde{\boldsymbol{\varphi}}_{n-1}(\mathbf{x}+\mathbf{v}_n^{k+1})-s_{n-1}-\delta s_n^k}{T\circ\tilde{\boldsymbol{\varphi}}_{n-1}(\mathbf{x}+\mathbf{v}_n^{k})-s_{n-1}-\delta s_n^k}\cdot(2m_{n-1}+2\delta m_n^k+2\ln D-2\ln T_n^{k+1}\\
&\quad+\ln\frac{T\circ\tilde{\boldsymbol{\varphi}}_{n-1}(\mathbf{x}+\mathbf{v}_n^{k+1})-s_{n-1}-\delta s_n^k}{T\circ\tilde{\boldsymbol{\varphi}}_{n-1}(\mathbf{x}+\mathbf{v}_n^{k})-s_{n-1}-\delta s_n^k})d\mathbf{x}\\
&\quad+\frac{1}{2\theta_n}\int_\Omega(\mathbf{v}_n^k-\mathbf{v}_n^{k+1})\cdot(\mathbf{v}_n^k+\mathbf{v}_n^{k+1}-2\mathbf{u}_n^k)d\mathbf{x}.
\end{aligned}
$$

By using Taylor's formula, we get

(3.10)
$$
\ln(T\circ\tilde{\boldsymbol{\varphi}}_{n-1}(\mathbf{x}+\mathbf{v}_n^{k+1})-s_{n-1}-\delta s_n^k)=\ln(T\circ\tilde{\boldsymbol{\varphi}}_{n-1}(\mathbf{x}+\mathbf{v}_n^{k})-s_{n-1}-\delta s_n^k)+A+B,
$$

where $A=\frac{\nabla_{\mathbf{v}}T\circ\tilde{\boldsymbol{\varphi}}_{n-1}(\mathbf{x}+\mathbf{v}_n^k)\cdot(\mathbf{v}_n^{k+1}-\mathbf{v}_n^k)}{T\circ\tilde{\boldsymbol{\varphi}}_{n-1}(\mathbf{x}+\mathbf{v}_n^k)-s_{n-1}-\delta s_n^k}$, $B=(\mathbf{v}_n^k-\mathbf{v}_n^{k+1})H(\sigma)(\mathbf{v}_n^k-\mathbf{v}_n^{k+1})^T$, and $H(\sigma)$ is the Hessian matrix of the function $\ln(T\circ\tilde{\boldsymbol{\varphi}}_{n-1}(\mathbf{x}+\mathbf{v}_n^k)-s_{n-1}-\delta s_n^k)$ on the point σ between $\mathbf{v}_n^k$ and $\mathbf{v}_n^{k+1}$. Note that here we use the condition $\alpha>3$ for technical demand to ensure $H_0^\alpha(\Omega)\hookrightarrow C^2(\Omega)$ (Theorem 4.58 in [9]). Due to $\boldsymbol{\varphi}_n\in[H_0^\alpha(\Omega)]^2$, we have $\tilde{\boldsymbol{\varphi}}_n\in[C^2(\Omega)]^2$, which implies $T\circ\boldsymbol{\varphi}_n\in C^2(\Omega)$. This makes the Hessian matrix $H(\cdot)$ of $T\circ\boldsymbol{\varphi}_n\in C^2(\Omega)$ well defined.

Hence, by (3.9) and (3.10), there holds

$$
\begin{aligned}
&E_n(\mathbf{v}_n^k,\mathbf{u}_n^k,\delta m_n^k,\delta s_n^k)-E_n(\mathbf{v}_n^{k+1},\mathbf{u}_n^k,\delta m_n^k,\delta s_n^k)\\
&\quad\ge\lambda_n\int_\Omega(A+B)^2d\mathbf{x}+c\|\mathbf{v}_n^{k+1}-\mathbf{v}_n^k\|^2_{[L^2(\Omega)]^2}+L(\mathbf{v}_n^k,\mathbf{v}_n^{k+1})\ge c\|\mathbf{v}_n^{k+1}-\mathbf{v}_n^k\|^2_{[L^2(\Omega)]^2},
\end{aligned}
$$

where $c=\frac{1}{2\theta_n}-c_0>0$ and $c_0=\|H(\sigma)\|_{L^\infty(\Omega)}=\frac{10\overline{M}^2(\lambda_n\widetilde{M})^n}{(\kappa-\kappa_0)^2}$ (see Appendix A for details). ∎

LEMMA 3.3. *For the subproblem* (3.4)*, there holds*

(3.11)
$$
\begin{aligned}
&2\mu\int_\Omega\nabla^\alpha\mathbf{u}_n^{k+1}\cdot\nabla^\alpha\mathbf{w}d\mathbf{x}+2\Theta\int_\Omega\left(\frac{\partial u_{n,1}^{k+1}}{\partial x_1}-\frac{\partial u_{n,2}^{k+1}}{\partial x_2}\right)\cdot\left(\frac{\partial w_1^{k+1}}{\partial x_1}-\frac{\partial w_2^{k+1}}{\partial x_2}\right)d\mathbf{x}\\
&\quad+2\Theta\int_\Omega\left(\frac{\partial u_{n,1}^{k+1}}{\partial x_2}+\frac{\partial u_{n,2}^{k+1}}{\partial x_1}\right)\cdot\left(\frac{\partial w_1^{k+1}}{\partial x_2}+\frac{\partial w_2^{k+1}}{\partial x_1}\right)d\mathbf{x}\\
&\quad-\frac{1}{\theta_n}\int_\Omega(\mathbf{v}_n^{k+1}-\mathbf{u}_n^{k+1})\cdot\mathbf{w}d\mathbf{x}=0
\end{aligned}
$$

for any $\mathbf{w}\in[C_0^\infty(\Omega)]^2$ *and*

$$
E_n(\mathbf{v}_n^{k+1},\mathbf{u}_n^k,\delta m_n^k,\delta s_n^k)-E_n(\mathbf{v}_n^{k+1},\mathbf{u}_n^{k+1},\delta m_n^k,\delta s_n^k)\ge c_1\|\mathbf{u}_n^k-\mathbf{u}_n^{k+1}\|^2_{[H_0^\alpha(\Omega)]^2}
$$

for some $c_1>0$.

Proof. The first-order variation of (3.4) is

$$
\begin{aligned}
&2\mu\int_\Omega \nabla^\alpha \mathbf{u}_n^{k+1}\cdot\nabla^\alpha \mathbf{w}d\mathbf{x}+2\Theta\int_\Omega\left(\frac{\partial u_{n,1}^{k+1}}{\partial x_1}-\frac{\partial u_{n,2}^{k+1}}{\partial x_2}\right)\cdot\left(\frac{\partial w_1^{k+1}}{\partial x_1}-\frac{\partial w_2^{k+1}}{\partial x_2}\right)d\mathbf{x}\\
&+2\Theta\int_\Omega\left(\frac{\partial u_{n,1}^{k+1}}{\partial x_2}+\frac{\partial u_{n,2}^{k+1}}{\partial x_1}\right)\cdot\left(\frac{\partial w_1^{k+1}}{\partial x_2}+\frac{\partial w_2^{k+1}}{\partial x_1}\right)d\mathbf{x}\\
&-\frac{1}{\theta_n}\int_\Omega(\mathbf{v}_n^{k+1}-\mathbf{u}_n^{k+1})\cdot\mathbf{w}d\mathbf{x}=0,
\end{aligned}
$$

where $\mathbf{w}=(w_1,w_2)^T$ is a test function. This concludes (3.11).

Letting $\mathbf{w}=\mathbf{u}_n^k-\mathbf{u}_n^{k+1}$, then there holds

(3.12)

$$
\begin{aligned}
\tilde{L}(\mathbf{u}_n^k,\mathbf{u}_n^{k+1})=&2\mu\int_\Omega\nabla^\alpha\mathbf{u}_n^{k+1}\cdot\nabla^\alpha(\mathbf{u}_n^k-\mathbf{u}_n^{k+1})d\mathbf{x}+\frac{1}{\theta_n}\int_\Omega(\mathbf{u}_n^{k+1}-\mathbf{v}_n^{k+1})\cdot(\mathbf{u}_n^k-\mathbf{u}_n^{k+1})d\mathbf{x}\\
&+2\Theta\int_\Omega\left(\frac{\partial u_{n,1}^{k+1}}{\partial x_1}-\frac{\partial u_{n,2}^{k+1}}{\partial x_2}\right)\left(\frac{\partial u_{n,1}^{k}}{\partial x_1}-\frac{\partial u_{n,2}^{k}}{\partial x_2}\right)d\mathbf{x}\\
&+2\Theta\int_\Omega\left(\frac{\partial u_{n,1}^{k+1}}{\partial x_2}+\frac{\partial u_{n,2}^{k+1}}{\partial x_1}\right)\left(\frac{\partial u_{n,1}^{k}}{\partial x_2}+\frac{\partial u_{n,2}^{k}}{\partial x_1}\right)d\mathbf{x}\\
&-2\Theta\int_\Omega\left(\frac{\partial u_{n,1}^{k+1}}{\partial x_1}-\frac{\partial u_{n,2}^{k+1}}{\partial x_2}\right)^2d\mathbf{x}-2\Theta\int_\Omega\left(\frac{\partial u_{n,1}^{k+1}}{\partial x_2}+\frac{\partial u_{n,2}^{k+1}}{\partial x_1}\right)^2d\mathbf{x}=0.
\end{aligned}
$$

Therefore, based on (3.12), we obtain

$$
\begin{aligned}
&E_n(\mathbf{v}_n^{k+1},\mathbf{u}_n^k,\delta m_n^k,\delta s_n^k)-E_n(\mathbf{v}_n^{k+1},\mathbf{u}_n^{k+1},\delta m_n^k,\delta s_n^k)\\
&\quad\ge\mu\|\nabla^\alpha(\mathbf{u}_n^k-\mathbf{u}_n^{k+1})\|^2_{[L^2(\Omega)]^2}+\frac{1}{2\theta_n}\|\mathbf{u}_n^k-\mathbf{u}_n^{k+1}\|^2_{[L^2(\Omega)]^2}+\tilde{L}(\mathbf{u}_n^k,\mathbf{u}_n^{k+1})\\
&\quad\ge c_1\|\mathbf{u}_n^k-\mathbf{u}_n^{k+1}\|^2_{[H_0^\alpha(\Omega)]^2}.
\end{aligned}
\tag{3.13}
$$

∎

Lemma 3.4. *For subproblems* (3.5) *and* (3.6)*, there holds*

$$
2\lambda_n(m_{n-1}+\delta m_n^{k+1}+\ln D-\ln T_n^{k+1})-\mu\mathrm{div}\left(\frac{\delta m_n^{k+1}}{|\delta m_n^{k+1}|}\right)=0,
\tag{3.14}
$$

$$
2\lambda_n(m_{n-1}+\delta m_n^{k+1}+\ln D-\ln \tilde{T}_n^{k+1})\frac{1}{\tilde{T}_n^{k+1}}-\mu\mathrm{div}\left(\frac{\nabla\delta s_n^{k+1}}{|\nabla\delta s_n^{k+1}|}\right)=0,
\tag{3.15}
$$

(3.16)

$$
E_n(\mathbf{v}_n^{k+1},\mathbf{u}_n^{k+1},\delta m_n^k,\delta s_n^k)-E_n(\mathbf{v}_n^{k+1},\mathbf{u}_n^{k+1},\delta m_n^{k+1},\delta s_n^k)\ge\lambda_n\|\delta m_n^k-\delta m_n^{k+1}\|^2_{L^2(\Omega)},
$$

and

(3.17)

$$
E_n(\mathbf{v}_n^{k+1},\mathbf{u}_n^{k+1},\delta m_n^{k+1},\delta s_n^k)-E_n(\mathbf{v}_n^{k+1},\mathbf{u}_n^{k+1},\delta m_n^{k+1},\delta s_n^{k+1})\ge\lambda_n\|\delta s_n^k-\delta s_n^{k+1}\|^2_{L^2(\Omega)},
$$

where $\tilde{T}_n^{k+1}=T\circ\tilde{\boldsymbol{\varphi}}_{n-1}(\mathbf{x}+\mathbf{v}_n^{k+1})-s_{n-1}-\delta s_n^{k+1}$.

Proof. The first-order variation of (3.5) is

$$2\lambda_n \int_\Omega (m_{n-1} + \delta m_n^{k+1} + \ln D - \ln T_n^{k+1}) \cdot p d\mathbf{x} + \mu \int_\Omega \frac{\nabla \delta m_n^{k+1} \cdot \nabla p}{|\nabla \delta m_n^{k+1}|} d\mathbf{x} = 0,$$

where p is the test function. By using the integration-by-parts formula [13], we get (3.14).

Letting $p = \delta m_n^k - \delta m_n^{k+1}$, we have

$$\begin{aligned}\hat{L} = 2\lambda_n &\int_\Omega [m_{n-1} + \delta m_n^{k+1} + \ln D - \ln T_n^{k+1}] \cdot (\delta m_n^k - \delta m_n^{k+1}) d\mathbf{x} \\ &+ \mu \int_\Omega \frac{\nabla \delta m_n^{k+1} \cdot \nabla (\delta m_n^k - \delta m_n^{k+1})}{|\nabla \delta m_n^{k+1}|} d\mathbf{x} = 0.\end{aligned}$$

Then we obtain

$$\begin{aligned}&E_n(\mathbf{v}_n^{k+1}, \mathbf{u}_n^{k+1}, \delta m_n^k, \delta s_n^k) - E_n(\mathbf{v}_n^{k+1}, \mathbf{u}_n^{k+1}, \delta m_n^{k+1}, \delta s_n^k) \\ &\quad \geq \lambda_n \|\delta m_n^k - \delta m_n^{k+1}\|^2_{L^2(\Omega)} + \hat{L} = \lambda_n \|\delta m_n^k - \delta m_n^{k+1}\|^2_{L^2(\Omega)}.\end{aligned}$$

Further, by giving similar analysis on the subproblem (3.6), we conclude (3.15) and (3.17). ∎

Now, based on Lemmas 3.2–3.4, we give the convergence result of the sequence $\{(\mathbf{v}_n^k, \mathbf{u}_n^k, \delta m_n^k, \delta s_n^k)\}$.

THEOREM 3.5. *Assume that the conditions in Lemmas* 3.2–3.4 *are satisfied; then the sequence* $\{(\mathbf{v}_n^k, \mathbf{u}_n^k, \delta m_n^k, \delta s_n^k)\}$ *generated by* (3.3)–(3.6) *converges to the solution of* (3.1) *when* $k \to +\infty$.

Proof. First, we claim that there exists $(\mathbf{v}_n, \mathbf{u}_n, \delta m_n, \delta s_n) \in [L^2(\Omega)]^2 \times [H_0^\alpha(\Omega)]^2 \times \mathcal{C}_\Omega \times SV_0(\Omega)$ such that

$$\begin{aligned}&\mathbf{v}_n^k \xrightarrow{k} \mathbf{v}_n \text{ in } [L^2(\Omega)]^2, \ \mathbf{u}_n^k \xrightarrow{k} \mathbf{u}_n \text{ in } [H_0^\alpha(\Omega)]^2, \\ &\delta m_n^k \xrightarrow{k} \delta m_n \text{ in } \mathcal{C}_\Omega, \ \delta s_n^k \xrightarrow{k} \delta s_n \text{ in } SV_0(\Omega).\end{aligned} \tag{3.18}$$

By Lemmas 3.2–3.4, we obtain that

$$\begin{aligned}&E_n(\mathbf{v}_n^k, \mathbf{u}_n^k, \delta m_n^k, \delta s_n^k) - E_n(\mathbf{v}_n^{k+1}, \mathbf{u}_n^{k+1}, \delta m_n^{k+1}, \delta s_n^{k+1}) \\ &\geq c\|\mathbf{v}_n^k - \mathbf{v}_n^{k+1}\|^2_{[L^2(\Omega)]^2} + c_1 \|\mathbf{u}_n^k - \mathbf{u}_n^{k+1}\|^2_{[H_0^\alpha(\Omega)]^2} \\ &\quad + \lambda_n \|\delta m_n^k - \delta m_n^{k+1}\|^2_{L^2(\Omega)} + \lambda_n \|\delta s_n^k - \delta s_n^{k+1}\|^2_{L^2(\Omega)}.\end{aligned} \tag{3.19}$$

Note that $E_n(\mathbf{v}_n^k, \mathbf{u}_n^k, \delta m_n^k, \delta s_n^k)$ is a decreasing sequence with a lower bound, which implies that the left side of (3.19) converges to zero when $k \to +\infty$. Hence, we have,

$$\begin{aligned}&\|\mathbf{v}_n^k - \mathbf{v}_n^{k+1}\|^2_{[L^2(\Omega)]^2} \xrightarrow{k} 0, \quad \|\mathbf{u}_n^k - \mathbf{u}_n^{k+1}\|^2_{[H_0^\alpha(\Omega)]^2} \xrightarrow{k} 0, \\ &\|\delta m_n^k - \delta m_n^{k+1}\|^2_{L^2(\Omega)} \xrightarrow{k} 0, \quad \|\delta s_n^k - \delta s_n^{k+1}\|^2_{L^2(\Omega)} \xrightarrow{k} 0,\end{aligned} \tag{3.20}$$

as $k \to +\infty$. Then by the compactness of Banach space $L^2(\Omega)$, $H_0^\alpha(\Omega)$, there exists $(\mathbf{v}_n, \mathbf{u}_n, \delta m_n, \delta s_n) \in [L^2(\Omega)]^2 \times [H_0^\alpha(\Omega)]^2 \times L^2(\Omega) \times L^2(\Omega)$ such that

$$\begin{aligned}&\mathbf{v}_n^k \xrightarrow{k} \mathbf{v}_n \text{ in } [L^2(\Omega)]^2, \ \mathbf{u}_n^k \xrightarrow{k} \mathbf{u}_n \text{ in } [H_0^\alpha(\Omega)]^2, \\ &\delta m_n^k \xrightarrow{k} \delta m_n \text{ in } L^2(\Omega), \ \delta s_n^k \xrightarrow{k} \delta s_n \text{ in } L^2(\Omega).\end{aligned}$$

In addition, since δm_n^k is bounded in $BV(\Omega)$, there exists a subsequence of δm_n^k which are still labeled with δm_n^k and $\delta \bar{m}_n \in BV_0(\Omega)$ such that

$$\|\delta m_n^k - \delta \bar{m}_n\|_{L^1(\Omega)} \xrightarrow{k} 0, \ \int_\Omega \nabla \delta m_n^k \cdot w d\mathbf{x} \xrightarrow{k} \int_\Omega \nabla \delta \bar{m}_n \cdot w d\mathbf{x}, \tag{3.21}$$

for any $w \in C_0^\infty(\Omega)$. By (3.20), (3.21), and the uniqueness of the limit for m_n^k, there holds $\delta m_n = \delta \bar{m}_n \in BV_0(\Omega)$. So we have $m_{n-1} + \delta m_n \in \mathcal{C}_\Omega$. Similarly, we also have $s_{n-1} + \delta s_n \in SV_0(\Omega)$. Therefore, we obtain the claim (3.18).

Next, we claim that $(\mathbf{v}_n, \mathbf{u}_n, \delta m_n, \delta s_n)$ is a minimizer of (3.1).

By (3.7), (3.11), and (3.18), we know that

$$-2\lambda_n[m_{n-1} + m_n + \ln D - \ln T_n]\frac{\nabla_{\mathbf{v}} T \circ \tilde{\boldsymbol{\varphi}}_{n-1}(\mathbf{x} + \mathbf{v}_n)}{T_n} + \frac{1}{\theta_n}(\mathbf{v}_n - \mathbf{u}_n) = 0 \tag{3.22}$$

and

$$\begin{aligned} &2\mu \int_\Omega \nabla^\alpha \mathbf{u}_n \cdot \nabla^\alpha \mathbf{z} d\mathbf{x} + 2\Theta \int_\Omega \left(\frac{\partial u_{n,1}}{\partial x_1} - \frac{\partial u_{n,2}}{\partial x_2}\right) \cdot \left(\frac{\partial z_1}{\partial x_1} - \frac{\partial z_2}{\partial x_2}\right) d\mathbf{x} \\ &\quad + 2\Theta \int_\Omega \left(\frac{\partial u_{n,1}}{\partial x_2} + \frac{\partial u_{n,2}}{\partial x_1}\right) \cdot \left(\frac{\partial z_1}{\partial x_2} + \frac{\partial z_2}{\partial x_1}\right) d\mathbf{x} - \frac{1}{\theta_n} \int_\Omega (\mathbf{v}_n - \mathbf{u}_n) \cdot \mathbf{z} d\mathbf{x} = 0, \end{aligned} \tag{3.23}$$

where $T_n = T \circ \tilde{\boldsymbol{\varphi}}_{n-1}(\mathbf{x} + \mathbf{v}_n) - s_{n-1} - \delta s_n$. By (3.14), we also obtain

$$2\lambda_n[m_{n-1} + \delta m_n^{k+1} + \ln D - \ln T_n^{k+1}] + \mathcal{H}(\delta m_n^{k+1}) = 0,$$

where $\mathcal{H}(m_n^{k+1}) = -\mu \mathrm{div}\left(\frac{\nabla \delta m_n^{k+1}}{|\nabla \delta m_n^{k+1}|}\right)$. This implies

$$\mathcal{H}(\delta m_n^{k+1}) \xrightarrow{k} -2\lambda_n[m_{n-1} + \delta m_n + \ln D - \ln T_n] \triangleq \mathcal{T}.$$

Note that $\mathcal{H}$ is a monotone operator because $\mathcal{H}$ is the derivative of a convex functional, which shows

$$\int_\Omega [\mathcal{H}(\delta m_n^{k+1}) - \mathcal{H}(\omega)] \cdot (\delta m_n^{k+1} - \omega) d\mathbf{x} \geq 0 \ \forall \omega \in BV(\Omega).$$

Furthermore, there holds

$$\int_\Omega \mathcal{H}(\delta m_n^{k+1}) \cdot \delta m_n^{k+1} d\mathbf{x} \xrightarrow{k} \int_\Omega \mathcal{T} \cdot \delta m_n d\mathbf{x},$$

and

$$\int_\Omega \mathcal{H}(\omega) \cdot \delta m_n^{k+1} d\mathbf{x} \xrightarrow{k} \int_\Omega \mathcal{H}(\omega) \cdot \delta m_n d\mathbf{x}.$$

So we get

$$\int_\Omega [\mathcal{T} - \mathcal{H}(\omega)] \cdot (\delta m_n - \omega) d\mathbf{x} \geq 0.$$

Let $\omega = \delta m_n + h\psi$ for any $\psi \in C_0^\infty(\Omega)$, and we have

$$\int_\Omega [\mathcal{T} - \mathcal{H}(\delta m_n + h\psi)] \cdot \psi d\mathbf{x} \leq 0.$$

Besides,

$$\int_\Omega \mathcal{H}(\delta m_n + h\psi)\cdot\psi d\mathbf{x} \longrightarrow \int_\Omega \mathcal{H}(\delta m_n)\cdot\psi d\mathbf{x}$$

as $h\to 0$. Therefore,

$$\int_\Omega \mathcal{T}\cdot\psi d\mathbf{x} \le \int_\Omega \mathcal{H}(\delta m_n)\cdot\psi d\mathbf{x}.$$

So we have $\mathcal{H}(\delta m_n)=\mathcal{T}$ and

$$2\lambda_n[m_{n-1}+\delta m_n+\ln D-\ln T_n]+\mathcal{H}(\delta m_n)=0. \tag{3.24}$$

In a similar way, there holds

$$2\lambda_n[m_{n-1}+\delta m_n+\ln D-\ln T_n]\frac{1}{T_n}-\mu\mathrm{div}\left(\frac{\nabla\delta s_n}{|\nabla\delta s_n|}\right)=0. \tag{3.25}$$

Then by (3.22), (3.23), (3.24), and (3.25), we conclude that $(\mathbf{v}_n,\mathbf{u}_n,\delta m_n,\delta s_n)$ is a minimizer of (3.1). ∎

At the end of this section, we focus on the numerical implementation of the subproblem (3.3)–(3.6). For some given domain $\Omega=(0,a)\times(0,a)$ and scale number n, we define $h=\frac{a}{N_S}$ for some given $N_S\in\mathbb{N}^+$. Here, we also define $(x_1)_i=ih$, $(x_2)_j=jh$ for $i,j=0,1,2,\ldots,N_S$ and $\mathbf{P}_{i,j}=((x_1)_i,(x_2)_j)$ for $i,j=0,1,2,\ldots,N_S$.

v-problem: Define $r(\mathbf{v})=m_{n-1}+\delta m_n^k+\ln D-\ln(T\circ\tilde{\boldsymbol{\varphi}}_{n-1}(\mathbf{x}+\mathbf{v}(\mathbf{x}))-s_{n-1}-\delta s_n^k)$. By using Taylor's formula, there holds

$$r(\mathbf{v}_n^{k+1})\approx r(\mathbf{u}_n^k)-\mathbf{L}^k\cdot(\mathbf{v}_n^{k+1}-\mathbf{u}_n^k), \tag{3.26}$$

where $\mathbf{L}^k=(L_x,L_y)^T=\frac{1}{T\circ\tilde{\boldsymbol{\varphi}}_{n-1}(\mathbf{x}+\mathbf{u}_n^k(\mathbf{x}))-s_{n-1}-\delta s_n^k}\nabla_{\mathbf{u}}T\circ\tilde{\boldsymbol{\varphi}}_{n-1}(\mathbf{x}+\mathbf{u}_n^k(\mathbf{x}))$. Substituting (3.26) into (3.3), we obtain the following Euler–Lagrange equation for (3.3)

$$\mathbf{G}\mathbf{v}_n^{k+1}=\boldsymbol{\phi}(\mathbf{u}_n^k)\ \forall\mathbf{x}\in\Omega, \tag{3.27}$$

where

$$\mathbf{G}=\begin{pmatrix}1+2\lambda_{n-1}\theta_n L_x^2, & 2\lambda_{n-1}\theta_n L_xL_y\\ 2\lambda_{n-1}\theta_n L_xL_y, & 1+2\lambda_{n-1}\theta_n L_y^2\end{pmatrix},\ \mathbf{v}_n^{k+1}=\begin{pmatrix}v_{n,1}^{k+1}\\ v_{n,2}^{k+1}\end{pmatrix},$$

$$\boldsymbol{\phi}(\mathbf{u}_n^k)=\begin{pmatrix}u_{n,1}^k+2\lambda_{n-1}\theta_n[r(\mathbf{u}_n^k)L_x+L_x^2u_{n,1}^k+L_xL_yu_{n,2}^k]\\ u_{n,2}^k+2\lambda_{n-1}\theta_n[r(\mathbf{u}_n^k)L_y+L_xL_yu_{n,1}^k+L_y^2u_{n,2}^k]\end{pmatrix},$$

and $\mathbf{u}_n^k\triangleq(u_{n,1}^k,u_{n,2}^k)^T$. By solving the linear system (3.27), one gets the updated $\mathbf{v}_n^{k+1}$ for each $\mathbf{x}\in\Omega$.

u-problem: Based on the updated $\mathbf{v}_n^{k+1}$, the Euler–Lagrange equation for $\mathbf{u}$ from (3.4) is formulated as follows:

$$2\mu\theta_n\mathrm{div}^{\alpha*}(\nabla^\alpha\mathbf{u}_n^{k+1})-2\Theta\theta_n\triangle\mathbf{u}_n^{k+1}+\mathbf{u}_n^{k+1}=\mathbf{v}_n^{k+1}\ \forall\mathbf{x}\in\Omega. \tag{3.28}$$

Concerning the numerical computation of (3.28), the multigrid method is used to accelerate the algorithm. The details of the multigrid method for (3.28) are listed in Algorithm B.1 in Appendix B.

***m*-problem:** By ignoring the constant term, (3.5) is essentially equivalent to the following convex optimization problem:

$$\delta m_n^{k+1} = \underset{m_{n-1}+m\in\mathcal{C}_\Omega}{\arg\min} \ \frac{1}{2}\int_\Omega |g-m|^2 d\mathbf{x} + \frac{\mu}{2\lambda_{n-1}}\int_\Omega |\nabla m| d\mathbf{x} \ \forall \mathbf{x}\in\Omega, \tag{3.29}$$

where $g(\mathbf{x}) = \ln(T\circ\tilde{\boldsymbol{\varphi}}_{n-1}(\mathbf{x}+\mathbf{v}^{k+1}) - s_{n-1}(\mathbf{x}) - \delta s_n^k(\mathbf{x})) - m_{n-1}(\mathbf{x}) - \ln D(\mathbf{x})$. Without the constraint $K_1 \le m \le K_2$, (3.29) is essentially a standard form of the total variation minimization. The solution of (3.29) (without constraint $K_1 \le m \le K_2$) is

$$m = g - \mathcal{P}_{\lambda K}(g). \tag{3.30}$$

Note that here and in what follows, $\mathcal{P}_A(v)$ denotes the element in A which minimizes the distance between v and all the elements in A. Here we use the Chambolle Projection algorithm [2] to compute $\mathcal{P}_{\lambda K}(g)$. By giving the initial value $\mathbf{p}^0 = (0,0)$, $0 < \tau < \frac{1}{8}$, and the iterative sequence

$$\mathbf{p}_{i,j}^{l+1} = \frac{\mathbf{p}^l + \tau\nabla(\mathrm{div}\mathbf{p}^l - g/\lambda)_{i,j}}{1+\tau|\nabla(\mathrm{div}\mathbf{p}^l - g/\lambda)_{i,j}|},$$

we have $\lambda \mathrm{div}\mathbf{p}^l \to \mathcal{P}_{\lambda K}(g)$ with $l \to +\infty$ [2]. Then, based on (3.30), we get the solution of (3.29) by projecting the solution of (3.30) onto the set $\mathcal{C}_\Omega$:

$$(\delta m_n^{k+1})_{i,j} = \begin{cases} [g-\mathcal{P}_{\lambda K}(g)]_{i,j}, & K_1 \le [g-\mathcal{P}_{\lambda K}(g)]_{i,j} \le K_2, \\ K_1, & [g-\mathcal{P}_{\lambda K}(g)]_{i,j} < K_1, \\ K_2, & [g-\mathcal{P}_{\lambda K}(g)]_{i,j} > K_2, \end{cases} \tag{3.31}$$

for $i,j = 0,1,2,\ldots,N_S$.

***s*-problem:** Define $\mathcal{G}(\Omega) = \{s \in BV_0(\Omega) | s(\mathbf{x}) \le \kappa - \kappa_0 - s_{n-1}(\mathbf{x}) \ \ \forall\, \mathbf{x}\in\Omega\}$. Then $\mathcal{G}(\Omega)$ is a closed and convex set. Assume that δs_n is a solution of (3.4). Then for any $r \in \mathcal{G}(\Omega)$, there holds $\delta s_n + \tau(r - \delta s_n) = (1-\tau)\delta s_n + \tau r \in \mathcal{G}(\Omega)$ for $0 \le \tau \le 1$. Next, we define $J(\tau) = E_n(\mathbf{v}_n^{k+1}, \mathbf{u}_n^{k+1}, \delta m_n^{k+1}, \delta s_n + \tau(r - \delta s_n))$, which yields

$$J(0) \le J(\tau) \ \forall \tau \in [0,1].$$

Therefore,

$$0 \le J'(0) = \int_\Omega \mathcal{F}(\delta s_n)\cdot(r - \delta s_n) d\mathbf{x} \ \ \forall\ r \in \mathcal{G}, \tag{3.32}$$

where $\mathcal{F}(\delta s_n) = \frac{2\lambda_n(m_{n-1}+\delta m_n^{k+1} + \ln D - \ln(T\circ\tilde{\boldsymbol{\varphi}}_{n-1}(\mathbf{x}+\mathbf{v}_n^{k+1}) - s_{n-1} - \delta s_n))}{T\circ\tilde{\boldsymbol{\varphi}}_{n-1}(\mathbf{x}+\mathbf{v}_n^{k+1}) - s_{n-1} - \delta s_n} - \mu\mathrm{div}(\frac{\nabla\delta s_n}{|\nabla\delta s_n|})$. Note that $\mathcal{F}$ is a monotone operator [22], and (3.32) is equivalent to $\delta s_n = \mathcal{P}_{\mathcal{G}}[\delta s_n - \varrho\mathcal{F}(\delta s_n)]$, which induces the following iterative method for (3.4):

$$\delta s_n^{l+1} = \mathcal{P}_{\mathcal{G}}[\delta s_n^l - \varrho\mathcal{F}(\delta s_n^l)],\ l = 0,1,2,\ldots, \tag{3.33}$$

with $\varrho > 0$. Concerning the projection in (3.33), it is essential to solve the following optimization problem:

$$(\delta s_n^{l+1})_{i,j} = \arg\min_{w_{i,j}} \|[\delta s_n^l - \varrho\mathcal{F}(\delta s_n^l)]_{i,j} - w_{i,j}\|^2,$$

subject to $w_{i,j} \le \kappa - \kappa_0 - (s_{n-1})_{i,j}$ for $i,j = 0,1,2,\ldots,N_S$. That is,

Algorithm 3.1 ADM for (3.1).

Initialization: $k=0$, $\mathbf{u}_n^0=\mathbf{0}$, $\mathbf{v}_n^0=\mathbf{0}$, $m_n^0=0$, $s_n^0=0$, Ω and maximum iteration times K.
while $k\le K$ **do**
Step 1. Update $\mathbf{v}_n^{k+1}$ by (3.27);
Step 2. Update $\mathbf{u}_n^{k+1}$ by (3.28);
Step 3. Update δm_n^{k+1} by (3.31);
Step 4. Update δs_n^{k+1} by (3.34);
Set $k=k+1$;
end while
Output: $\mathbf{u}_n=\mathbf{u}_n^K$,$\mathbf{v}_n=\mathbf{v}_n^K$, $\delta m_n=\delta m_n^K$, $\delta s_n=\delta s_n^K$.

Algorithm 3.2 Multiscale algorithm for (2.1)–(2.2).

Initialization: $n=0$, $\mathbf{u}_n^0=\mathbf{0}$, $\mathbf{v}_n^0=\mathbf{0}$, $\delta m_n^0=0$, $\delta s_n^0=0$, λ_n, $\theta_n(n=0,1,2,\dots,N)$, Θ and maximum scale N.
while the scale number $n\le N$ **do**
Step 1. Use Algorithm 3.1 to compute $\mathbf{v}_n$ (cf. (3.27)), $\mathbf{u}_n$ (cf. (3.28)), δm_n (cf. (3.31)), and δs_n (cf. (3.34)) on Ω;
Step 2. Compute $\tilde{\boldsymbol{\varphi}}_n$, m_n, and s_n on Ω;
Set $n=n+1$ and go to the next scale with a different value for λ_n (multiscale for parameter λ_n);
end while
Output: $\tilde{\boldsymbol{\varphi}}_N$, m_N, s_N.

$$(\delta s_n^{l+1})_{i,j}=\begin{cases}[\delta s_n^l-\varrho\mathcal{F}(\delta s_n^l)]_{i,j}, & [\delta s_n^l-\varrho\mathcal{F}(s_n^l)]_{i,j}\le\kappa-\kappa_0-(s_{n-1})_{i,j},\\ \kappa-\kappa_0-(s_{n-1})_{i,j}, & [\delta s_n^l-\varrho\mathcal{F}(\delta s_n^l)]_{i,j}>\kappa-\kappa_0-(s_{n-1})_{i,j},\end{cases}\tag{3.34}$$

for $i,j=0,1,2,\dots,N_S$.

To summarize the above details, an ADM algorithm for solving (3.1) is listed in Algorithm 3.1. Furthermore, based on Algorithm 3.1, we propose Algorithm 3.2 to implement the multiscale approach (2.1)–(2.2), which will be refined later from the viewpoint of the multiresolution.

4. Coarse-to-fine strategy for the multiscale approach. To solve the multiscale approach (2.1)–(2.2), one needs to iteratively solve the subproblems (3.3)–(3.6) for each scale n (see Algorithm 3.2 for details). This strategy is not yet efficient. Based on the viewpoint of the multiresolution, we now propose a modified coarse-to-fine strategy for the numerical implementation of the multiscale approach (2.1)–(2.2). This strategy contains the following two steps (the flow chart of the proposed coarse-to-fine strategy is displayed in Figure 5). Note that here and in what follows, $\Omega\downarrow 2^n$ denotes the downsampling of the region Ω with size 2^n. For example, given the region $\Omega=(0,128)\times(0,128)$, $\Omega\downarrow 2^1$ denotes the region $(0,64)\times(0,64)$).

(I) Image decomposition: To improve the resolution of downsampled images, image decomposition process is additionally introduced. Here, the decomposition model we used is the canonical multiscale image decomposition model developed by [32, 35], which is essentially based on the following definite partial differential equation (PDE) problem:

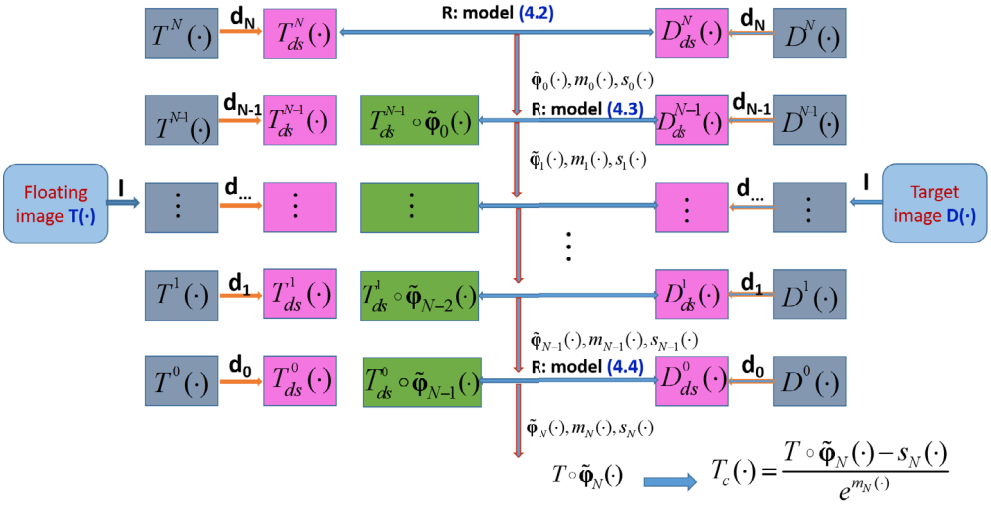

FIG. 5. *The flow chart of the proposed coarse-to-fine strategy for the joint diffeomorphic image registration and intensity correction. Note that here* **I** *denotes the image decomposition process;* **R** *denotes the image registration process;* **d** *denotes the downsampling process.*

$$
\begin{cases}
\dfrac{\partial \xi(\mathbf{x},t)}{\partial t} = \rho(t)\mathrm{div}\left(\dfrac{\delta(\mathbf{x})\nabla\xi(\mathbf{x},t)}{|\nabla\xi(\mathbf{x},t)|}\right), & \mathbf{x}\in\Omega, t>0,\\
\xi(\mathbf{x},0) = f(\mathbf{x}), & \mathbf{x}\in\overline{\Omega},\\
\xi(\mathbf{x},t)\,|_{\mathbf{x}\in\partial\Omega} = 0, & t>0,
\end{cases} \tag{4.1}
$$

where we set $\rho(t) = 1.05^t$, $\delta(\mathbf{x}) = \frac{1}{\sqrt{1+|\nabla(G_\iota * f)(\mathbf{x})|^2/\beta^2}}$, $\beta = 0.07$, and G_ι is a Gaussian kernel with a small standard deviation ι. By choosing $N+1$ different time points $0 = t_0 < t_1 < \cdots < t_N$ and setting $f = T$ or $f = D$, we obtain the image decomposition results: T^N, T^{N-1}, ..., T^0 and D^N, D^{N-1}, ..., D^0, respectively. Concerning the numerical implementation of (4.1), one can refer to [35] for details. Therefore, we downsample the decomposed images $T^n(\cdot), D^n(\cdot)$ $(n = 0,1,2,\ldots,N)$ with size 2^n to obtain the downsampled images $T^n_{ds}(\cdot)$ and $D^n_{ds}(\cdot)$, respectively.

Remark 4.1. (4.1) is a multiscale process for image decomposition, which acts as a role of smoothing image if the image pair $T(\cdot), D(\cdot)$ are of low resolutions. In fact, under the situation where the image pair $T(\cdot), D(\cdot)$ are of high resolutions, we can omit the image decomposition and downsample the image pair into image sequences $T^n(\cdot), D^n(\cdot)$ $(n = 0,1,2,\ldots,N)$ directly.

(II) Image registration: The coarse-to-fine strategy for a multiscale approach of joint image registration and intensity correction model is divided into the following $N+1$ steps, here and in what follows, $\Omega_n = \Omega \downarrow 2^{N-n} (n = 0,1,2,\ldots,N)$.

Step 0. By taking $T^N_{ds}(\cdot)$ and $D^N_{ds}(\cdot)$ as the floating image and target image, respectively, we solve the following variational problem on Ω_0:

$$
(\mathbf{u}_0, \delta m_0, \delta s_0) \in \underset{(\mathbf{u},m,s)\in\mathcal{L}_{\varepsilon_0}(\Omega_0)}{\arg\min} \widetilde{J}_0(\mathbf{u}, m, s), \tag{4.2}
$$

where $\widetilde{J}_0(\mathbf{u},m,s) = \lambda_0 \int_{\Omega_0} (m(\mathbf{x}) + \ln D^N_{ds}(\mathbf{x}) - \ln(T^N_{ds}(\mathbf{x}+\mathbf{u}(\mathbf{x})) - s(\mathbf{x})))^2 d\mathbf{x} + \mu R_{\Omega_0}(\mathbf{u},m,s)$, $\mathcal{L}_{\varepsilon_0}(\Omega_0) = (\mathcal{A}(\Omega_0)\setminus\mathcal{B}_{\varepsilon_0}(\Omega_0)) \times \mathcal{C}_{\Omega_0} \times SV_0(\Omega_0)$, and $\varepsilon_0 > 0$. $R_{\Omega_n}(\mathbf{u},m,s)$

is defined by replacing Ω with Ω_n in (1.3). Define $\tilde{\boldsymbol{\varphi}}_0(\mathbf{x}) = \boldsymbol{\varphi}_0(\mathbf{x}) = \mathbf{x} + \mathbf{u}_0(\mathbf{x})$, $m_0(\mathbf{x}) = \delta m_0(\mathbf{x})$, and $s_0(\mathbf{x}) = \delta s_0(\mathbf{x})$ for each $\mathbf{x} \in \Omega_0$.

Step 1. Scale $\tilde{\boldsymbol{\varphi}}_0(\mathbf{x})$, $m_0(\mathbf{x})$, and $s_0(\mathbf{x})$ to Ω_1 and solve the following variational problem on Ω_1 (note that here $|\Omega_1| = 4|\Omega_0|$):

$$(\mathbf{u}_1, \delta m_1, \delta s_1) \in \underset{(\mathbf{u}, m_0+m, s_0+s)\in\mathcal{L}_{\varepsilon_1}(\Omega_1)}{\arg\min} \widetilde{J}_1(\mathbf{u}, m, s), \tag{4.3}$$

where $\widetilde{J}_1(\mathbf{u}, m, s) = \lambda_1 \int_{\Omega_1} (m_0(\mathbf{x}) + m(\mathbf{x}) + \ln D_{ds}^{N-1}(\mathbf{x}) - \ln(T_{ds}^{N-1} \circ \tilde{\boldsymbol{\varphi}}_0(\mathbf{x} + \mathbf{u}(\mathbf{x})) - s_0(\mathbf{x}) - s(\mathbf{x})))^2 d\mathbf{x} + \mu R_{\Omega_1}(\mathbf{u}, m, s)$, $\mathcal{L}_{\varepsilon_1}(\Omega_1) = (\mathcal{A}(\Omega_1) \setminus \mathcal{B}_{\varepsilon_1}(\Omega_1)) \times \mathcal{C}_{\Omega_1} \times SV_0(\Omega_1)$, and $\varepsilon_1 > 0$. Define $\boldsymbol{\varphi}_1(\mathbf{x}) = \mathbf{x} + \mathbf{u}_1(\mathbf{x})$, $\tilde{\boldsymbol{\varphi}}_1(\mathbf{x}) = \tilde{\boldsymbol{\varphi}}_0 \circ \boldsymbol{\varphi}_1(\mathbf{x})$, $m_1(\mathbf{x}) = m_0(\mathbf{x}) + \delta m_1(\mathbf{x})$, and $s_1(\mathbf{x}) = s_0(\mathbf{x}) + \delta s_1(\mathbf{x})$ for each $\mathbf{x} \in \Omega_1$.

$$\vdots$$

Step N. Scale $\tilde{\boldsymbol{\varphi}}_{N-1}(\mathbf{x})$, $m_{N-1}(\mathbf{x})$, and $s_{N-1}(\mathbf{x})$ to Ω_N, and solve the following variational problem on Ω_N (note that $\Omega_N = \Omega$):

$$(\mathbf{u}_N, \delta m_N, \delta s_N) \in \underset{(\mathbf{u}, m_{N-1}+m, s_{N-1}+s)\in\mathcal{L}_{\varepsilon_N}(\Omega_N)}{\arg\min} \widetilde{J}_N(\mathbf{u}, m, s), \tag{4.4}$$

where $\widetilde{J}_N(\mathbf{u}, m, s) = \lambda_n \int_{\Omega_N} (m_{N-1}(\mathbf{x}) + m(\mathbf{x}) + \ln D(\mathbf{x}) - \ln(T \circ \tilde{\boldsymbol{\varphi}}_{N-1}(\mathbf{x} + \mathbf{u}(\mathbf{x})) - s_{N-1}(\mathbf{x}) - s(\mathbf{x})))^2 d\mathbf{x} + \mu R_{\Omega_N}(\mathbf{u}, m, s)$, $\mathcal{L}_{\varepsilon_N}(\Omega_N) = (\mathcal{A}(\Omega_N) \setminus \mathcal{B}_{\varepsilon_N}(\Omega_N)) \times \mathcal{C}_{\Omega_N} \times SV_0(\Omega_N)$, and $\varepsilon_N > 0$. Define $\boldsymbol{\varphi}_N(\mathbf{x}) = \mathbf{x} + \mathbf{u}_N(\mathbf{x})$, $\tilde{\boldsymbol{\varphi}}_N(\mathbf{x}) = \tilde{\boldsymbol{\varphi}}_{N-1} \circ \boldsymbol{\varphi}_N(\mathbf{x})$, $m_N(\mathbf{x}) = m_{N-1}(\mathbf{x}) + \delta m_N(\mathbf{x})$, and $s_N(\mathbf{x}) = s_{N-1}(\mathbf{x}) + \delta s_N(\mathbf{x})$.

To show the convergence of the above proposed coarse-to-fine strategy, we introduce some notations. In the coarse-to-fine strategy, one needs to scale the functions $\boldsymbol{\varphi}^{\Omega_n} : \Omega_n \to \Omega_n$, $m^{\Omega_n} : \Omega_n \to \mathbb{R}$, $s^{\Omega_n} : \Omega_n \to \mathbb{R}$ and $\mathbf{u}^{\Omega_n} : \Omega_n \to \mathbb{R}$ to the functions $\boldsymbol{\varphi} : \Omega \to \Omega$, $m : \Omega \to \mathbb{R}$, $s : \Omega \to \mathbb{R}$, and $\mathbf{u} : \Omega \to \mathbb{R}$, respectively. By the principle of scaling, there holds $\boldsymbol{\varphi}(\mathbf{y}) = 2^{N-n}\boldsymbol{\varphi}^{\Omega_n}(\frac{\mathbf{y}}{2^{N-n}})$, $\mathbf{u}(\mathbf{y}) = 2^{N-n}\mathbf{u}^{\Omega_n}(\frac{\mathbf{y}}{2^{N-n}})$, $m(\mathbf{y}) = m^{\Omega_n}(\frac{\mathbf{y}}{2^{N-n}})$, and $s(\mathbf{y}) = s^{\Omega_n}(\frac{\mathbf{y}}{2^{N-n}})$, where $\mathbf{y} \in \Omega$ and $\mathbf{x} = \mathbf{y}/2^{N-n} \in \Omega_n$. Here, functions $f_{\Omega_n}(f = \boldsymbol{\varphi}, m, s, \mathbf{u})$ denote the version of the function f on the domain Ω_n. In addition, there also holds $T_{ds}^n(\frac{\mathbf{y}}{2^{N-n}}) = T(\mathbf{y})$ and $D_{ds}^n(\frac{\mathbf{y}}{2^{N-n}}) = D(\mathbf{y})$.

Based on these notations, we have the following results.

THEOREM 4.2. *For any $n \le N-1$, the coarse level registration problem*

$$(\mathbf{u}_n^{\Omega_n}, \delta m_n^{\Omega_n}, \delta s_n^{\Omega_n}) \in \underset{(\mathbf{u}^{\Omega_n}, m^{\Omega_{n-1}}+m^{\Omega_n}, s^{\Omega_{n-1}}+s^{\Omega_n})\in\mathcal{L}_{\varepsilon_n}(\Omega_n)}{\arg\min} \widetilde{E}_n(\mathbf{u}^{\Omega_n}, m^{\Omega_n}, s^{\Omega_n}) \tag{4.5}$$

is equivalent to the variational problem

$$(\mathbf{u}_n, \delta m_n, \delta s_n) \in \underset{(\mathbf{u}, m_n+m, s_n+s)\in\mathcal{L}_{\varepsilon_n}(\Omega)}{\arg\min} \overline{E}_n(\mathbf{u}, m, s), \tag{4.6}$$

where $\widetilde{E}_n(\mathbf{u}, m, s) = \lambda_n \int_{\Omega_n} (m_{n-1}^{\Omega_n}(\mathbf{x}) + m^{\Omega_n}(\mathbf{x}) + \ln D_{ds}^{N-n}(\mathbf{x}) - \ln(T_{ds}^{N-n} \circ \tilde{\boldsymbol{\varphi}}_{n-1}^{\Omega_n}(\mathbf{x} + \mathbf{u}^{\Omega_n}(\mathbf{x})) - s_{n-1}^{\Omega_n}(\mathbf{x}) - s^{\Omega_n}(\mathbf{x})))^2 d\mathbf{x} + \mu R_{\Omega_n}(\mathbf{u}^{\Omega_n}, m^{\Omega_n}, s^{\Omega_n})$, $\overline{E}_n(\mathbf{u}, m, s) = 4^{N-n}\lambda_n \int_{\Omega} (m_{n-1}(\mathbf{x}) + m(\mathbf{x}) + \ln D_{ds}^{N-n}(\mathbf{x}) - \ln(T_{ds}^{N-n} \circ \tilde{\boldsymbol{\varphi}}_{n-1}(\mathbf{x} + \mathbf{u}(\mathbf{x})) - s_{n-1}(\mathbf{x}) - s(\mathbf{x})))^2 d\mathbf{x} + \mu(R_{1,\Omega}(\mathbf{u}) + 2^{N-n}(R_{2,\Omega}(m) + R_{3,\Omega}(s)))$.

Proof. By letting $\mathbf{y} = 2^{N-n}\mathbf{x} \in \Omega$ for any $\mathbf{x} \in \Omega_n$, we get

$$\begin{aligned}
&\widetilde{E}_n(\mathbf{u}^{\Omega_n}, m^{\Omega_n}, s^{\Omega_n}) \\
&\quad = \frac{1}{4^{N-n}}\lambda_n \int_{\Omega} (m_{n-1}(\mathbf{y}) + m(\mathbf{y}) + \ln D_{ds}^{N-n}(\mathbf{y}) - \ln(T_{ds}^{N-n} \circ \tilde{\boldsymbol{\varphi}}_{n-1}(\mathbf{y} + \mathbf{u}(\mathbf{y})) \\
&\qquad - s_{n-1}(\mathbf{y}) - s(\mathbf{y})))^2 d\mathbf{y} + \frac{\mu}{16^{N-n}}(R_{1,\Omega}(\mathbf{u}) + 2^{N-n}(R_{2,\Omega}(m) + R_{3,\Omega}(s))).
\end{aligned}$$

Therefore, (4.5) is equivalent to (4.6). ∎

Algorithm 4.1 Coarse-to-fine algorithm for the multiscale approach (4.2)–(4.4).

Initialization: $n=0$, $\mathbf{u}_n^0=\mathbf{0}$, $\mathbf{v}_n^0=\mathbf{0}$, $m_n^0=0$, $s_n^0=0$, λ_n, θ_n $(n=0,1,2,\ldots,N)$, Θ and maximum scale N.

I: Image decomposition:

Solve the image decomposition model (4.1) by setting $f=T$ and D to obtain the decomposition result; Downsample the decomposed images T^n, D^n $(n=0,1,2,\ldots,N)$ with size 2^n to obtain the downsampled images $T_{ds}^n(\cdot)$ and $D_{ds}^n(\cdot)$, respectively.

II: Image registration:

while $n<N$ **do**

Step 1. Use Algorithm 3.1 to compute $\mathbf{v}_n$ (cf. (3.27)), $\mathbf{u}_n$ (cf. (3.28)), δm_n (cf. (3.31)), and δs_n (cf. (3.34)) on Ω_n and replace $T(\cdot)$, $D(\cdot)$ with $T_{sd}^{N-n}(\cdot)$, $D_{sd}^{N-n}(\cdot)$, respectively;

Step 2. Compute $\tilde{\boldsymbol{\varphi}}_n$, m_n, and s_n on Ω_n;

Step 3. Scale the definition of $\tilde{\boldsymbol{\varphi}}_n$, m_n, and s_n onto a finer domain Ω_{n+1}; Set $n=n+1$;

end while

Output: $\tilde{\boldsymbol{\varphi}}_N$,$m_N$, s_N and $T_c(\cdot)=\frac{T\circ\tilde{\boldsymbol{\varphi}}_N(\cdot)-s_N(\cdot)}{e^{m_N(\cdot)}}$.

By Theorem 4.2, the variational problem (4.2)–(4.4) on each coarse grid is equivalent to the following variational problem:

$$(\mathbf{u}_n,\delta m_n,\delta s_n)\in \underset{(\mathbf{u},m_{n-1}+m,s_{n-1}+s)\in\mathcal{L}_{\varepsilon_n}(\Omega)}{\arg\min} \overline{E}_n(\mathbf{u},m,s),\quad n=0,1,2,\ldots,N. \tag{4.7}$$

Then based on Theorems 4.2 and 2.6, we give the following convergence result of the proposed coarse-to-fine strategy (4.2)–(4.4).

THEOREM 4.3. *Let $\tilde{\boldsymbol{\varphi}}_n$ and m_n, s_n $(n=0,1,2,\ldots,N)$ be induced by the multiscale approach* (4.2)–(4.4). *Assume three large numbers B, M, λ_n satisfy $\lim_{n\to N^-,N\to+\infty}\frac{B^{4n-3}M^{4^n}}{\lambda_n}=0$, where B is a positive number depending on Ω and M is a positive number depending on $\mathbf{u}_0$, δm_0, δs_0, Ω, α, and ϕ, respectively. Then there holds $\phi=\delta$; i.e., the modified coarse-to-fine strategy* (4.2)–(4.4) *is also equivalent to the original greedy matching problem* (2.17).

Proof. Based on Theorem 4.2, we can transform the variational problems (4.2)–(4.4) into an equivalent problem (4.7), which is defined on Ω. Further, one can notice that (4.7) is equivalent to (2.2) with $n\to N^-$. Therefore, we can use Theorem 2.6 to show $\phi=\delta$. ∎

Based on Algorithm 3.1, the proposed coarse-to-fine strategy for the multiscale approach (4.2)–(4.4) is summarized in Algorithm 4.1.

Remark 4.4. Algorithm 4.1 is a multiresolution modification for Algorithm 3.2. In Algorithm 3.2, we need to solve the variational problem on Ω, while in Algorithm 4.1, we just need to solve the same problem on $\Omega_n(n=0,1,2,\ldots,N)$. By $|\Omega_n|=\frac{1}{4^{N-n}}|\Omega|$, we know that Algorithm 4.1 accelerates Algorithm 3.2, which will be validated in section 5. In addition, by Theorem 4.2, the scale n of the coarse-to-fine approach (4.2)–(4.4) is equivalent to the scale n of the non–coarse-to-fine approach (4.7), whatever the region Ω is downsampled. Hence, the downsampling process does not affect the final result when n is large enough.

5. Applications for the proposed multiscale approach. In this section, we perform three different kinds of numerical tests to validate the theoretical results and algorithms in sections 2–4. The content of this section contains: In the test of subsection 5.2, we perform the comparison between the proposed coarse-to-fine Algorithm 4.1 and multiscale 2D fractional-order diffeomorphic image registration (M2FDIR) in [20] to show that Algorithm 4.1 is more efficient on addressing the image registration problem with local varying illumination. In the test of subsection 5.3, a comparison between Algorithm 4.1 and Algorithm 3.2 is performed to show that the proposed Algorithm 4.1 has advantage on reducing the CPU consumption. In the subsection 5.4 test, the proposed Algorithm 4.1 is compared with some state-of-the-art image registration algorithms, including 1D fast diffeomorphic image registration [17], diffeomorphic fractional-order image registration algorithm (DFIRA) [18], large deformation diffeomorphic metric mapping (LDDMM) [25], and forward–backward Nash equilibrium (FBNE) [33]. All the numerical tests are performed under Windows 7 and MATLAB R2012b with Intel core i7-6700 CPU @3.40GHz and 8GB memory. For the quantitative comparison, we choose the following two indices:

- Relative sum of squared differences (Re_SSD) defined by

$$\text{Re\_SSD}(T, D, \mathbf{u}) = \frac{\text{SSD}(T(\mathbf{x}+\mathbf{u}), D)}{\text{SSD}(T, D)},$$

  where $\text{SSD}(T, D) = \frac{1}{2}\sum_{i,j}(T_{i,j} - D_{i,j})^2$.
- Mesh folding number (MFN) defined by

$$\text{MFN}(\mathbf{u}) = \sharp\left(\det \overline{J}(\mathbf{u}) \le 0\right),$$

  where $\det \overline{J}(\mathbf{u}) = (1+\frac{\partial u_1}{\partial x_1})(1+\frac{\partial u_2}{\partial x_2}) - \frac{\partial u_1}{\partial x_2}\frac{\partial u_2}{\partial x_1}$, and for any set A, $\sharp(A)$ denotes the number of elements in A.

5.1. Sensitivity test for parameters $\boldsymbol{\lambda_n}$ and $\boldsymbol{\mu}$ in Algorithm 4.1. λ_n and μ are two key parameters for Algorithm 4.1. To show the sensitivity of the sequence $\{\lambda_n\}$ and the parameter μ, the synthetic image pair (pair I) is used as the testing data. For pair I, the floating image and target image are defined as follows:

$$T(\mathbf{x}) = 255\chi_{\bar{\Gamma}_1}(\mathbf{x}) + 0.01,\ D(\mathbf{x}) = 255\chi_{\bar{\Gamma}_2}(\mathbf{x}) + 100\chi_{\bar{\Gamma}_3}(\mathbf{x}) + 0.01,$$

where $\Omega = (0,128)\times(0,128)$, $\bar{\Gamma}_1 = \{\mathbf{x} = (x_1,x_2)^T : (x_1-65)^2 + (x_2-65)^2 \le 40^2\}$, $\bar{\Gamma}_2 = \{\mathbf{x} = (x_1,x_2)^T : (x_1-65)^2 + (x_2-65)^2 < 10^2\}$, $\bar{\Gamma}_3 = \{\mathbf{x} = (x_1,x_2)^T : 10^2 \le (x_1-65)^2 + (x_2-65)^2 \le 20^2\}$, and χ is an indicator function. The original synthetic image pair is shown in Figure 6.

By setting $\lambda_n = \lambda_0 \times 4^n (n = 0,1,2,\ldots)$, $\mu \in [0.01, 1000]$, and $\lambda_0 \in [15000, 100000]$, we use Algorithm 4.1 to perform the registration for image pair I by giving 357 different groups (only 132 groups are shown on Figure 7 to make the vision more plausible) of λ_0 and μ. By viewing the final $\text{Re\_SSD}(T, D, \mathbf{u})$ as the heat value, the heat map for λ_0 and μ is shown in Figure 7.

According to Figure 7, we find that the final $\text{Re\_SSD}(T, D, \mathbf{u})$ is not affected by the parameters λ_n and μ. This validates that the multiscale approach (2.1)–(2.2) can provide a solution to the greedy matching problem (2.17), which has nothing to do with the parameters λ_n and μ.

5.2. Comparison between the proposed coarse-to-fine Algorithm 4.1 and M2FDIR in [20]. To show that the proposed model via (4.2)–(4.4) properly treats the local varying illumination, we compare the proposed Algorithm 4.1 with

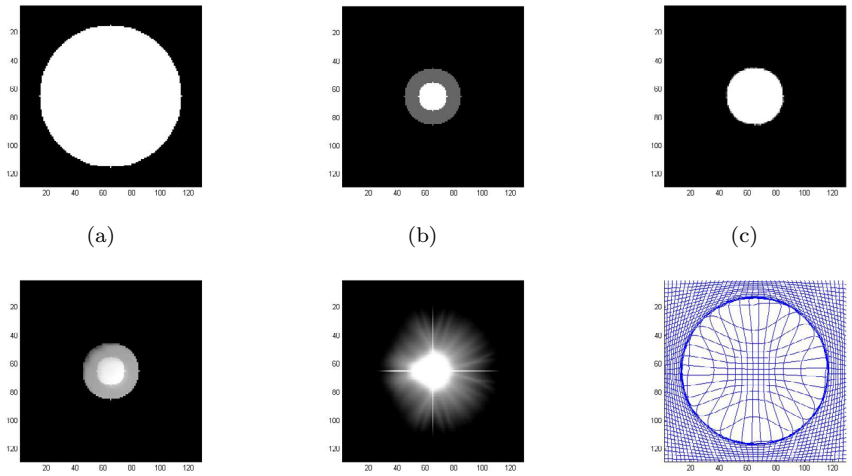

FIG. 6. *Comparison on pair* I*:* (a) *floating image* $T(\cdot)$*;* (b) *target image* $D(\cdot)$*;* (c) $T \circ \tilde{\boldsymbol{\varphi}}_N(\cdot)$ *in Algorithm* 4.1*,* Re_SSD=5.14%*;* (d) $T_c \circ \tilde{\boldsymbol{\varphi}}_N(\cdot)$ *in Algorithm* 4.1,Re_SSD=0.89%*;* (e) $T \circ \tilde{\boldsymbol{\varphi}}_{K_M}(\cdot)$ *in M2FDIR* [20]*,* Re_SSD=7.65%*;* (f) *mesh grid of the deformation* $\tilde{\boldsymbol{\varphi}}_N(\cdot)$ *in Algorithm* 4.1.

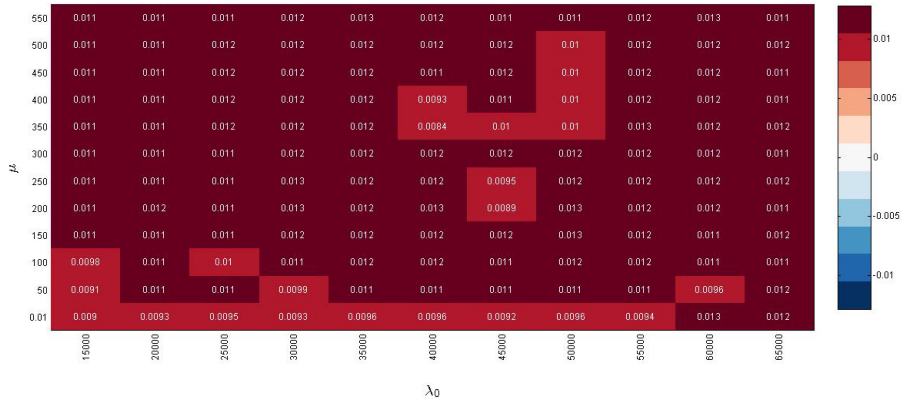

FIG. 7. *The heat map for* λ_0 *and* μ*. The values in the table are* $\text{Re\_SSD}(T, D, \mathbf{u})$ *with respect to different* λ_0 *and* μ*.*

the multiscale M2FDIR in [20], which does not take the local varying illumination into consideration. The test pair in this part contains synthetic image pair I and two brain MRI image pairs (II–III) with local varying illumination.

For pair I, one can see from Figure 6 that there is a shadow on the outer ring of the circle in the target image $D(\cdot)$, while no shadow appears in the floating image $T(\cdot)$. By using image pair I, we use the proposed Algorithm 4.1 and M2FDIR in [20] for registration. The final registration results and quantitative comparison are listed in Figure 6 and Table 1. By Figure 6(f), one can notice that the proposed Algorithm 4.1 produces a diffeomorphic deformation $\boldsymbol{\varphi}$. It follows from Figure 6(d) that the registration result of Algorithm 4.1 matches the shadow ring of the target image $D(\cdot)$ well, while the final result of M2FDIR has trouble in matching the shadow ring. Besides, M2FDIR leads to a wrong result because of the distortion of the shadow ring in target image $D(\cdot)$. This shows the necessity to introduce the bias m, s in

TABLE 1
Quantitative comparison between registration results of Algorithm 4.1 *and M2FDIR (subsection* 5.2 *test).*

Data	Algorithm	Re-SSD(%)	MFN	CPU/s
Pair I	M2FDIR [20]	7.65	0	469.3
	Algorithm 4.1	**0.89**	**0**	**37.1**
Pair II	M2FDIR [20]	46.86	0	536.1
	Algorithm 4.1	**11.82**	**0**	**36.1**
Pair III	M2FDIR [20]	9.91	0	661.3
	Algorithm 4.1	**3.11**	**0**	**43.1**

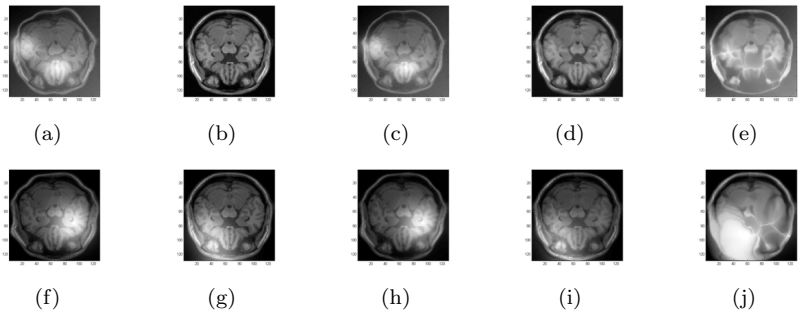

FIG. 8. *Comparison on pair* II *(First row):* (a) *floating image* $T(\cdot)$*;* (b) *target image* $D(\cdot)$*;* (c) $T \circ \tilde{\boldsymbol{\varphi}}_N(\cdot)$ *in Algorithm* 4.1, Re_SSD=85.31%*;* (d) $T_c \circ \tilde{\boldsymbol{\varphi}}_N(\cdot)$ *in Algorithm* 4.1,Re_SSD=11.82%*;* (e) $T \circ \tilde{\boldsymbol{\varphi}}_{K_M}(\cdot)$ *in M2FDIR* [20], Re_SSD=46.86%. *Comparison on pair* III *(Second row):* (f) *floating image* $T(\cdot)$*;* (g) *target image* $D(\cdot)$*;* (h) $T \circ \tilde{\boldsymbol{\varphi}}_N(\cdot)$ *in Algorithm* 4.1, Re_SSD=86.04%*;* (i) $T_c \circ \tilde{\boldsymbol{\varphi}}_N(\cdot)$ *in Algorithm* 4.1, Re_SSD=3.11%*;* (j) $T \circ \tilde{\boldsymbol{\varphi}}_{K_M}(\cdot)$ *in M2FDIR* [20], Re_SSD=9.91%*;*

variational model (1.3) and also validates that the proposed Algorithm 4.1 addresses the image registration with local illumination well.

For pair II (see the first row of Figure 8), there are two domains suffering from local varying illumination on the lower left of the floating image $T(\cdot)$, while no illumination appears in the target image $D(\cdot)$. For pair III (see the second row of Figure 8), there is local illumination on the right side of the floating image $T(\cdot)$, while local illumination appears on the opposite side of the target image $D(\cdot)$. We use Algorithm 4.1 and M2FDIR for pairs II and III. The results are shown in Figure 8 and the quantitative comparison results are listed in Table 1.

By Figure 8(e), we see that the registration result of M2FDIR on pair II is disturbed by the local varying illumination and leads to an unexpected result. In addition, one can notice from Figure 8(d) that the proposed Algorithm 4.1 addresses the local varying illumination well. This validates that the proposed Algorithm 4.1 has advantage on addressing the registration with local varying illumination over M2FDIR, which is also the main motivation for us to study the problem joint diffeomorphic image registration and intensity correction. Concerning the comparison on pair III, it follows from Figure 8(j) that the registration result is seriously bad in the region with local varying illumination, while the proposed Algorithm 4.1 can accurately correct the intensity distortion caused by the local illumination (see Figure 8(i) for details). In addition, in pair II and III, one can notice that the final Re_SSD of M2FDIR is smaller than the Re_SSD ($T \circ \tilde{\boldsymbol{\varphi}}_N(\cdot)$ in Algorithm 4.1) before intensity correction. This improvement in Re_SSD is meaningless since the pursuit of a smaller Re_SSD leads to a wrong deformation (seriously bad in the local illumination region). Lastly, one can notice from the registration result of Algorithm 4.1 (Figure 8(f)–(j)) that there is still local varying illumination to coincide with the target image. That is,

local varying illumination still cannot be recovered well if there is local varying illumination in target image $D(\cdot)$. This validates the fact in Remark 1.3 that the fidelity in (1.3) is formulated based on the assumption that the target image $D(\cdot)$ has no bias.

5.3. Comparison between the proposed coarse-to-fine Algorithm 4.1 and Algorithm 3.2 (without coarse-to-fine process). To solve the proposed multiscale approach (2.1)–(2.2), one has two choices: (1) Use the proposed Algorithm 3.2 without coarse-to-fine strategy. For this choice, one is expected to implement the ADM process (4.2)–(4.4) on Ω for each scale n. (2) Use the proposed coarse-to-fine Algorithm 4.1. For this choice, one only needs to solve the ADM process (4.2)–(4.4) on Ω_n for each scale n. Note that Ω_n is a domain smaller than Ω, which indicates that the proposed coarse-to-fine strategy (4.2)–(4.4) has advantage on reducing the CPU consumption over Algorithm 3.2.

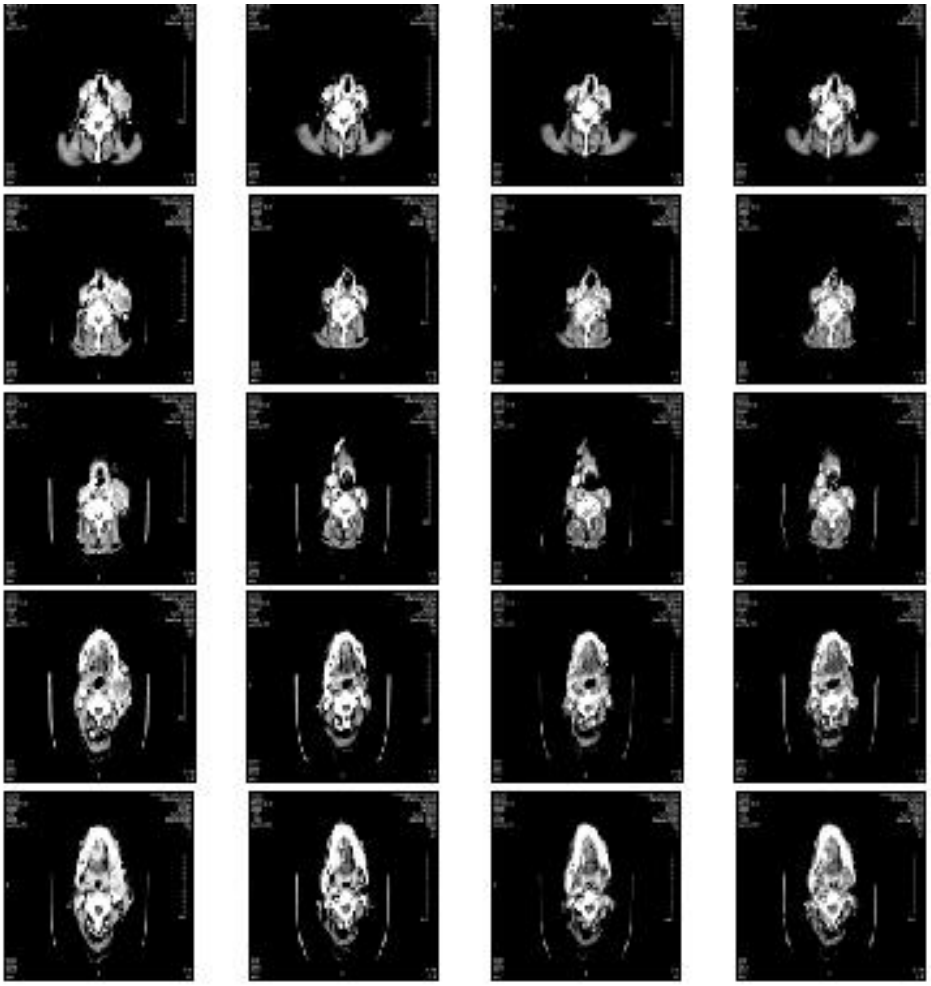

FIG. 9. *Comparison on* IV*: The first column is the floating image $T(\cdot)$ for each image pair; the second column is the floating image $D(\cdot)$ for each image pair; the third and fourth columns are the image registration results of Algorithm* 4.1 *and Algorithm* 3.2 *for each image pair, respectively.*

To numerically validate this theoretical result, we perform the comparison between Algorithm 4.1 and Algorithm 3.2. Both two algorithms aim to find the solution of the multiscale approach (2.1)–(2.2), where the coarse-to-fine strategy is introduced in Algorithm 4.1, but no multiresolution based coarse-to-fine strategy is used in Algorithm 3.2. The data set used for the test are labeled IV–VI. For pair IV, it contains five image pairs which are collected at two different time from one patient (no. 1) who suffers from the mouth cavity lymphoma. Similarly, data V and VI contain the same content from other two patients (no. 2 and no. 3). By registering these image pairs, clinicians can extract useful information from the difference between the deformed image $T_c \circ \tilde{\boldsymbol{\varphi}}_N(\cdot)$ and the target image $D(\cdot)$. Furthermore, by analyzing the difference, some evaluation for the severeness of the tumor is made. Therefore, the accuracy of the image registration result is of vital importance for the evaluation. Here, we use Algorithm 4.1 and Algorithm 3.2 to register these 15 image pairs. The registration results for IV–VI are listed on Figures 9–11 and Table 2, where Re_SSD is represented

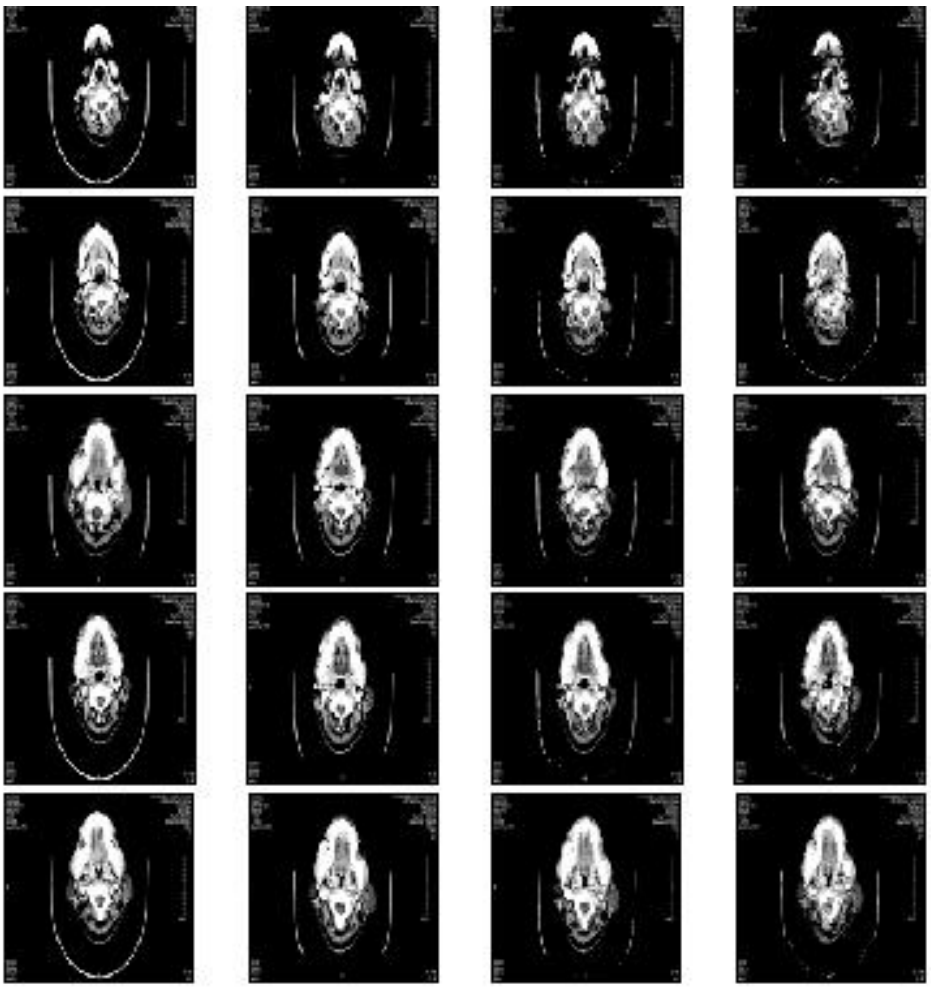

FIG. 10. *Comparison on* V*: The first column is the floating image* $T(\cdot)$ *for each image pair; the second column is the floating image* $D(\cdot)$ *for each image pair; the third and fourth columns are the image registration results of Algorithm* 4.1 *and Algorithm* 3.2 *for each image pair, respectively.*

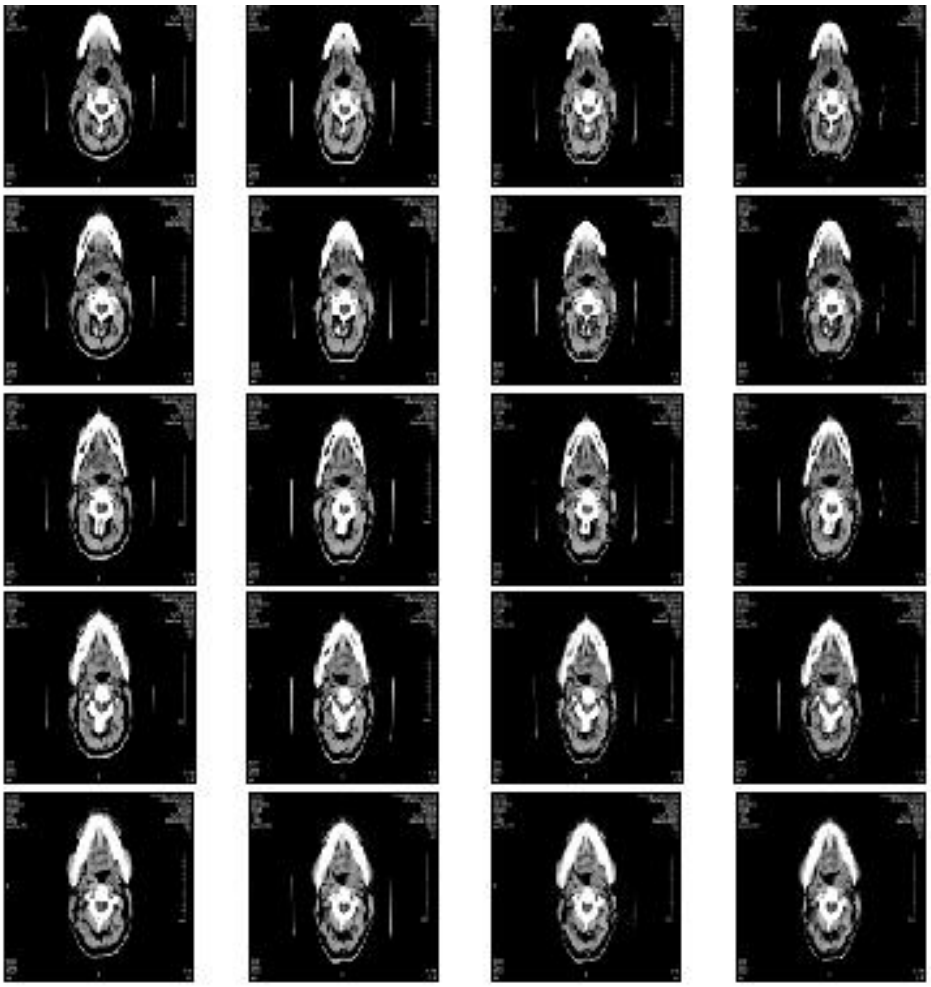

FIG. 11. *Comparison on* VI*: The first column is the floating image $T(\cdot)$ for each image pair; the second column is the floating image $D(\cdot)$ for each image pair; the third and fourth columns are the image registration results of Algorithm* 4.1 *and Algorithm* 3.2 *for each image pair, respectively.*

TABLE 2

Quantitative comparison between registration results of Algorithm 4.1 *and Algorithm* 3.2 *(subsection* 5.3 *test).*

Data	Algorithm	Re_SSD(%)	MFN	CPU/s
Data IV	**Algorithm 4.1**	10.67 ± 2.47	**0**	38.5 ± 5.3
	Algorithm 3.2	11.19 ± 3.44	0	518.5 ± 31.9
Data V	**Algorithm 4.1**	9.82 ± 2.47	**0**	36.1 ± 6.1
	Algorithm 3.2	13.16 ± 3.51	0	436.7 ± 35.6
Data VI	**Algorithm 4.1**	8.96 ± 1.68	**0**	43.1 ± 3.8
	Algorithm 3.2	12.76 ± 0.72	0	621.7 ± 45.6

by the mean value $\pm$ standard deviation of five different image pairs for each patient, and the CPU is represented in a similar way.

By Table 2, we see that the registration result of the proposed Algorithm 4.1 is similar to (though a bit better than) Algorithm 3.2. However, the CPU consumption

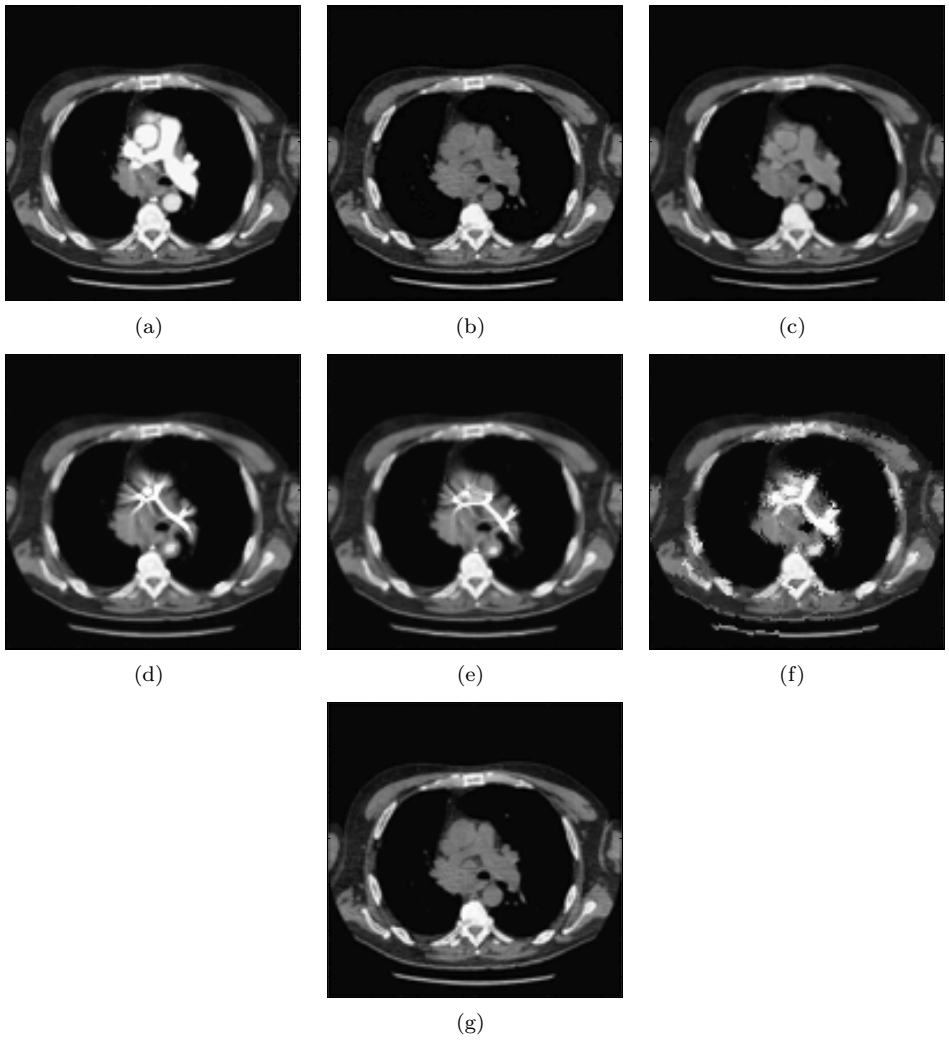

FIG. 12. *Comparison on* VII*:* (a) *floating image* $T(\cdot)$*;* (b) *target image* $D(\cdot)$*;* (c) $T \circ \tilde{\boldsymbol{\varphi}}_N(\cdot)$ *in Algorithm* 4.2*,* Re_SSD=9.76%*;* (d) 1*DFDIM,* Re_SSD=25.72%*;* (e) *DFIRA,* Re_SSD=22.8%*;* (f) *LDDMM,* Re_SSD=50.05%*;* (g) *FBNE,* Re_SSD=12.57%.

of Algorithm 4.1 is greatly reduced compared with Algorithm 3.2. This shows the efficiency of the proposed coarse-to-fine Algorithm 4.1.

5.4. Comparison between Algorithm 4.1 and some other image registration algorithms. In this part, to further validate the effectiveness and efficiency of the proposed coarse-to-fine Algorithm 4.1, we perform some comparisons between Algorithm 4.1 and 1DFDIM [17], DFIRA [18], LDDMM [25], and FBNE [33]. For this purpose, we use these five algorithms to match three different medical image pairs labeled with VII–IX. Here, VII–IX are kept the same state with data set used in [33], which are introduced as follows.

For image pair VII, the floating image $T(\cdot)$ contains a highly contrasted part in the middle of the region. By viewing the contrast as bias field relative to the target image $D(\cdot)$, the elimination of this kind of bias field provides a strong evidence that

TABLE 3
Quantitative comparisons between five different image registration algorithms.

Data	Algorithm	Re_SSD(%)	MFN	CPU/s
	Algorithm 4.1	**9.76**	**0**	**40.3**
	1DFDIM [17]	25.72	0	62.7
Ddata VII	DFIRA [18]	22.80	0	372.6
	LDDMM [25]	50.05	0	21.2
	FBNE [33]	12.57	0	118.6
	Algorithm 4.1	**5.28**	**0**	**42.2**
	1DFDIM [17]	76.09	0	86.3
Data VIII	DFIRA [18]	66.54	0	456.7
	LDDMM [25]	51.23	0	30.2
	FBNE [33]	24.41	0	101.6
	Algorithm 4.1	**3.05**	**0**	**50.4**
	1DFDIM [17]	83.2	0	90.3
Data IX	DFIRA [18]	68.96	0	748.4
	LDDMM [25]	36.18	0	23.7
	FBNE [33]	15.44	0	117.3

the proposed multiscale approach for the variational model joint image registration and intensity correction has advantage on addressing the diffeomorphic registration with local varying illumination. This is the main reason why these image pairs are selected for the numerical comparison. The quantitative comparison results for image pair VII are listed in Figure 12 and Table 3. One can notice from Figure 12 that only the proposed algorithm and the FBNE in [33] eliminate the bias field in the middle of the region well. The other three algorithms which do not take intensity correction into consideration lead to a narrow white bias field. This phenomenon occurs due to the minimization of the similarity $S(\mathbf{u})$. These solutions are not expected in image registration of image pair VII, which shows that the necessity for introducing the intensity correction process in the proposed Algorithm 4.1. Note that [33] pursuits a minimizer of the cost functional with three different regularizations, while Algorithm 4.1 searches for the minimizer of $S(\mathbf{u}, m, s)$ without any regularization. The comparison between Algorithm 4.1 and FBNE in [33] further validates the advantage of greedy matching. However, without proper multiscale consideration, greedy matching without regularization is not expected to work well, which illustrates that why the multiscale approach is introduced in this paper.

For image pair VIII, there is a low contrast in some local region of the floating image $T(\cdot)$, which may make it ineffective for some image registration models without intensity correction process. The registration result for image pair VIII is listed in Figure 13 and Table 3. The proposed algorithm and FBNE [33] successfully recover the low contrast region and lead to a final result with more details on the tissue. This shows the importance of intensity correction in the registration for these image pairs with a low contrast floating image. In this view, it is helpful to use the proposed algorithm to register the image pairs containing at least one high resolution image and one low contrast image. In addition, one can notice from Table 3 that the proposed Algorithm 4.1 achieves the best result for image pair VIII.

For image pair IX, the floating image contains bias field and varying illumination on different regions of the domain. Compared with image pair II used in the subsection 5.2 test, there is a square shadow surrounding the brain, which may affect the registration result. By Figure 14, we see that the local bias and square shadow

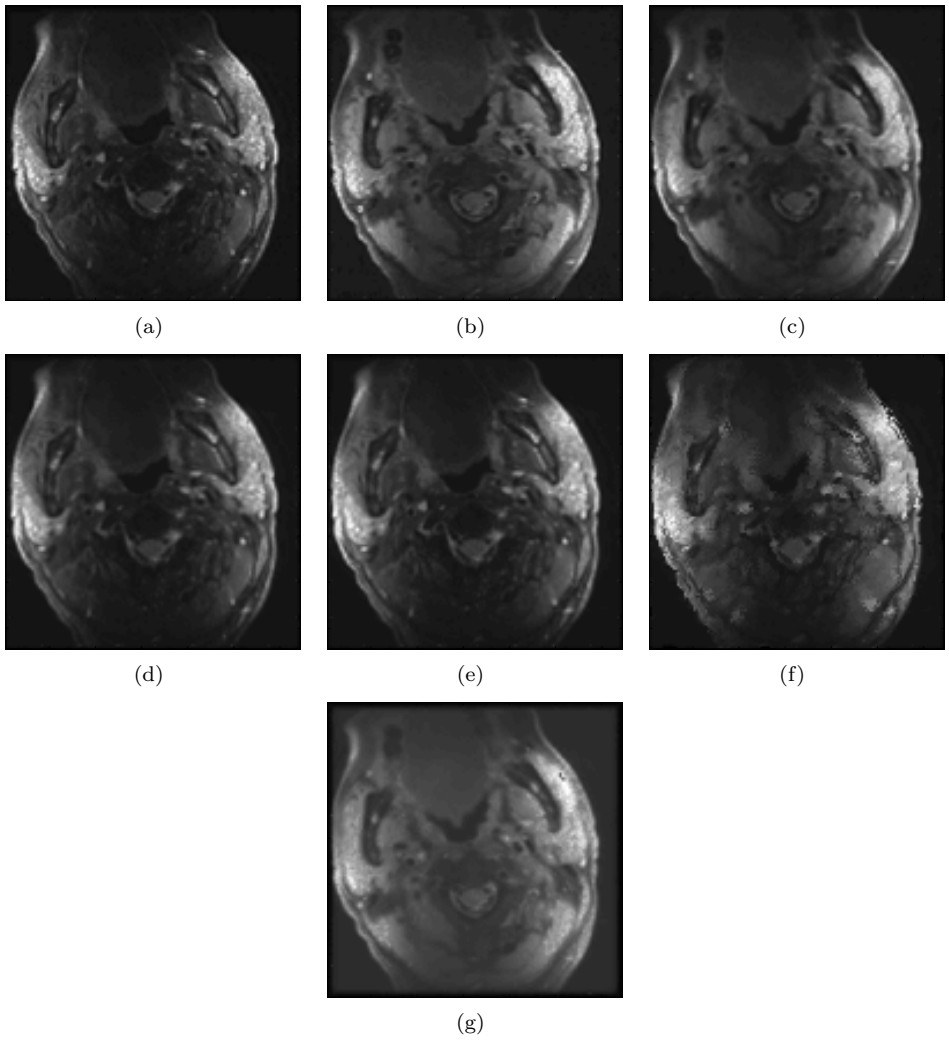

FIG. 13. *Comparison on* VIII*:* (a) *floating image* $T(\cdot)$*;* (b) *target image* $D(\cdot)$*;* (c) $T \circ \tilde{\varphi}_N(\cdot)$ *in Algorithm* 4.1*,* Re_SSD=5.28%*;* (d) 1*DFDIM,* Re_SSD=76.09%*;* (e) *DFIRA,* Re_SSD=66.54%*;* (f) *LDDMM,* Re_SSD=51.23%*;* (g) *FBNE,* Re_SSD=24.41%.

are well eliminated in the final result of the proposed Algorithm 4.1 and FBNE. This is an advantage led by bias correction in the proposed Algorithm 4.1 and FBNE. Moreover, by the quantitative comparisons on Table 3, one can see that the proposed Algorithm 4.1 achieves a smaller Re_SSD than FBNE.

6. Discussion.

6.1. Advantages of the multiscale approach. To address the intensity inhomogeneity in image registration, a state-of-the-art model was proposed by Theljani and Chen [33]. Furthermore, by using the Nash game theory, an iterative algorithm (FBNE) is also proposed based on the original variational model. However, under the framework of the Nash game theory, the final solution may be not the solution of the original variational model. This raises the uncertainty of the solution. In this paper,

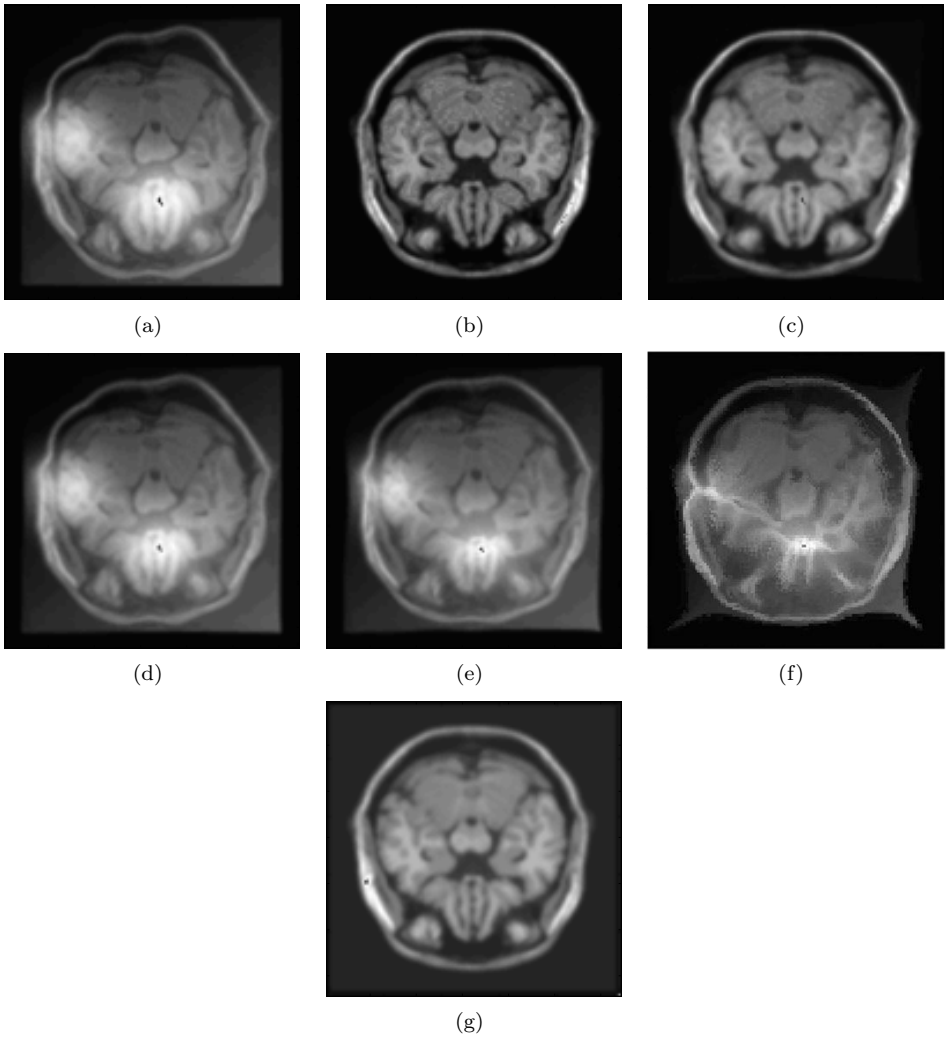

FIG. 14. *Comparison on* IX*:* (a) *floating image* $T(\cdot)$*;* (b) *target image* $D(\cdot)$*;* (c) $T \circ \tilde{\boldsymbol{\varphi}}_N(\cdot)$ *in Algorithm* 4.1*,* Re_SSD=3.05%*;* (d) 1*DFDIM,*Re_SSD=83.2%*;* (e) *DFIRA,* Re_SSD=68.96%*;* (f) *LDDMM,* Re_SSD=36.18%*;* (g) *FBNE,* Re_SSD=15.44%*.*

the proposed model (1.3) and related multiscale approach (2.1)–(2.2), aim at minimizing the similarity $S_{lc}(\mathbf{u}, m, s)$ on some smooth set $\mathcal{L}(\Omega)$, and achieve the solution of the greedy problem which joints image registration and intensity correction. This is also the reason why the proposed model achieves a better result than FBNE (see Figures 12–14 and Table 3).

6.2. Limitation. Although the proposed multiscale approach is capable of handling challenging image registration tasks such as large deformation and intensity inhomogeneity, we face the difficulties in scenario of occlusion or blur; see Figures 15 and 16 for details. The failure of Figures 15 and 16 may be due to the nonlocal intensity inhomogeneity of occlusion or blur (note the bias introduced in this paper is only capable of characterizing local intensity inhomogeneity). To address this challenge, some nonlocal methods are necessary to be introduced in image registration,

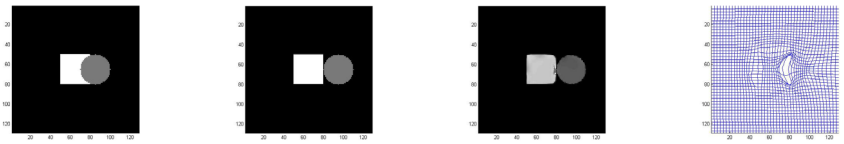

(a) (b) (c) (d)

FIG. 15. *Registration on occlusion:* (a) *floating image* $T(\cdot)$*;* (b) *target image* $D(\cdot)$*;* (c) *registration* $T_c \circ \tilde{\boldsymbol{\varphi}}_N(\cdot)$*;* (d) *deformation.*

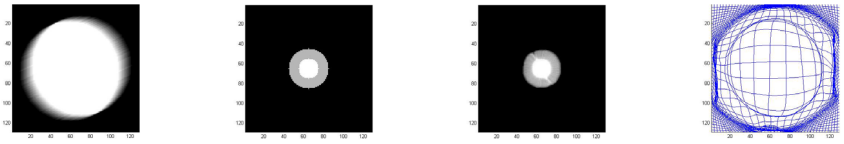

(a) (b) (c) (d)

FIG. 16. *Registration on blur:* (a) *floating image* $T(\cdot)$*;* (b) *target image* $D(\cdot)$*;* (c) *registration* $T_c \circ \tilde{\boldsymbol{\varphi}}_N(\cdot)$*;* (d) *deformation.*

for example, registration joint blind deblurring [26], and registration joint inpainting [37]. These may be new topics in registration with nonlocal intensity inhomogeneity.

7. Conclusion. In this paper, we propose a variational model for joint diffeomorphic image registration and intensity correction. Based on the joint model, a related greedy matching problem (2.17) is proposed. For solving the greedy matching problem (2.17), a multiscale approach is introduced to addresses the instability by directly solving the greedy matching problem (2.17), which provides a theoretical support for this kind of research. For the numerical computation of the multiscale approach, an ADM method is proposed and the convergence of this process is proved. In addition, a coarse-to-fine strategy is further introduced to accelerate the registration algorithm and its convergence is also established. Finally, three different kinds of numerical tests are performed to validate the theoretical results. For the future research, we may extend this work to the field of joint image registration and segmentation.

Appendix A. Estimation on the L^∞ norm for the Hessian matrix of $\ln(T\circ\tilde{\varphi}_{n-1}(x+v_n^k) - s_{n-1} - \delta s_n^k)$ with respect to v_n^k. The Hessian matrix of $\ln(T \circ \tilde{\boldsymbol{\varphi}}_{n-1}(\mathbf{x}+\mathbf{v}_n^k) - s_{n-1} - \delta s_n^k)$ is formulated as

$$H = \frac{1}{(T \circ \tilde{\boldsymbol{\varphi}}_{n-1}(\mathbf{x}+\mathbf{v}_n^k) - s_{n-1} - \delta s_n^k)^2} \begin{pmatrix} H_1 & H_2 \\ H_2 & H_3 \end{pmatrix},$$

where $H_1 = T\circ\tilde{\boldsymbol{\varphi}}_{n-1}(\mathbf{x}+\mathbf{v}_n^k)\frac{\partial^2}{\partial x_1^2}(T\circ\tilde{\boldsymbol{\varphi}}_{n-1}(\mathbf{x}+\mathbf{v}_n^k)) - (\frac{\partial}{\partial x_1}T\circ\tilde{\boldsymbol{\varphi}}_{n-1}(\mathbf{x}+\mathbf{v}_n^k))^2$, $H_2 = T\circ\tilde{\boldsymbol{\varphi}}_{n-1}(\mathbf{x}+\mathbf{v}_n^k)\frac{\partial^2}{\partial x_1 \partial x_2}(T\circ\tilde{\boldsymbol{\varphi}}_{n-1}(\mathbf{x}+\mathbf{v}_n^k)) - (\frac{\partial}{\partial x_1}T\circ\tilde{\boldsymbol{\varphi}}_{n-1}(\mathbf{x}+\mathbf{v}_n^k))(\frac{\partial}{\partial x_2}T\circ\tilde{\boldsymbol{\varphi}}_{n-1}(\mathbf{x}+\mathbf{v}_n^k))$, and $H_3 = T\circ\tilde{\boldsymbol{\varphi}}_{n-1}(\mathbf{x}+\mathbf{v}_n^k)\frac{\partial^2}{\partial x_2^2}(T\circ\tilde{\boldsymbol{\varphi}}_{n-1}(\mathbf{x}+\mathbf{v}_n^k)) - (\frac{\partial}{\partial x_2}T\circ\tilde{\boldsymbol{\varphi}}_{n-1}(\mathbf{x}+\mathbf{v}_n^k))^2$. By (1.3) and (3.6), we know $(T\circ\tilde{\boldsymbol{\varphi}}_{n-1}(\mathbf{x}+\mathbf{v}_n^k) - s_{n-1} - \delta s_n^k)^2 \geq (\kappa - \kappa_0)^2$.

Now we give an estimate on the L^∞ norm of H_1. Since $\alpha > 3$, by the Sobolev embddding Theorem [9] ($H_0^\alpha(\Omega) \hookrightarrow C^2(\Omega)$), we obtain

$$\begin{aligned}\|\nabla^2\boldsymbol{\varphi}\|^2_{C(\Omega)} = \|\nabla^2\mathbf{u}\|^2_{C(\Omega)} &\le CR_1(\mathbf{u}) \le C\lambda_n \int_\Omega (m_{n-1} + \ln D - \ln(T\circ\tilde{\boldsymbol{\varphi}}_{n-1} - s_{n-1}))^2 d\mathbf{x} \\ &\le 2C\lambda_n|\Omega|(K^2 + \ln^2(\overline{M}/\kappa)^2) \le \lambda_n\widetilde{M},\end{aligned}$$

where $\widetilde{M} \triangleq \widetilde{M}(\Omega,\alpha) = 2C|\Omega|(K^2 + \ln^2(\overline{M}/\kappa)^2) > 0$, and $C = C(\Omega,\alpha)$ is a positive constant (see Lemma 3.2 and Lemma 3.3 in [16] for details). Similarly, there holds

$$\|\mathbf{u}_n\|^2_{C^1(\Omega)} \le \lambda_n\widetilde{M}.$$

Note that

$$\nabla_{\mathbf{x}}\tilde{\boldsymbol{\varphi}}_n(\mathbf{x}) = \nabla_{\mathbf{g}_1}\boldsymbol{\varphi}_0 \cdot \nabla_{\mathbf{g}_2}\boldsymbol{\varphi}_1 \cdots \nabla_{\mathbf{g}_{n-1}}\boldsymbol{\varphi}_{n-2} \cdot \nabla_{\mathbf{g}_n}\boldsymbol{\varphi}_{n-1} \cdot \nabla_{\mathbf{x}}\boldsymbol{\varphi}_n(\mathbf{x}), \tag{A.1}$$

where $\mathbf{g}_k = \boldsymbol{\varphi}_k \circ \boldsymbol{\varphi}_2 \cdots \boldsymbol{\varphi}_n$ for $k = 1, 2, \ldots, n$. Since $\mathbf{g}_k$ are mappings from Ω to Ω, by (A.1), we obtain

$$\|\nabla_{\mathbf{x}}\tilde{\boldsymbol{\varphi}}_n(\mathbf{x})\|^2_{C(\Omega)} \le \lambda_0\lambda_1 \cdots \lambda_n\widetilde{M}^n \le (\lambda_n\widetilde{M})^n.$$

Then by the chain rule, we have

$$\frac{\partial T\circ\tilde{\boldsymbol{\varphi}}_{n-1}}{\partial x_1} = \frac{\partial T\circ\tilde{\boldsymbol{\varphi}}_{n-1}}{\partial\tilde{\varphi}^1_{n-1}}\frac{\partial\tilde{\varphi}^1_{n-1}}{\partial x_1} + \frac{\partial T\circ\tilde{\boldsymbol{\varphi}}_{n-1}}{\partial\tilde{\varphi}^2_{n-1}}\frac{\partial\tilde{\varphi}^2_{n-1}}{\partial x_1}$$

and

$$\begin{aligned}\frac{\partial^2 T\circ\tilde{\boldsymbol{\varphi}}_{n-1}}{\partial x_1^2} = &\frac{\partial^2 T\circ\tilde{\boldsymbol{\varphi}}_{n-1}}{\partial(\varphi^1_{n-1})^2}\left(\frac{\partial\varphi^1_{n-1}}{\partial x_1}\right)^2 + 2\frac{\partial^2 T\circ\tilde{\boldsymbol{\varphi}}_{n-1}}{\partial\varphi^1_{n-1}\partial\varphi^2_{n-1}}\frac{\partial\tilde{\varphi}^1_{n-1}}{\partial x_1}\frac{\partial\tilde{\varphi}^2_{n-1}}{\partial x_1}, \\ &+ \frac{\partial T\circ\tilde{\boldsymbol{\varphi}}_{n-1}}{\partial\tilde{\varphi}^2_{n-1}}\frac{\partial^2\tilde{\varphi}^2_{n-1}}{\partial x_1^2} + \frac{\partial^2 T\circ\tilde{\boldsymbol{\varphi}}_{n-1}}{\partial(\varphi^2_{n-1})^2}\left(\frac{\partial\varphi^2_{n-1}}{\partial x_1}\right)^2 \\ &+ \frac{\partial T\circ\tilde{\boldsymbol{\varphi}}_{n-1}}{\partial\tilde{\varphi}^1_{n-1}}\frac{\partial^2\tilde{\varphi}^1_{n-1}}{\partial x_1^2} + \frac{\partial T\circ\tilde{\boldsymbol{\varphi}}_{n-1}}{\partial\tilde{\varphi}^2_{n-1}}\frac{\partial^2\tilde{\varphi}^2_{n-1}}{\partial x_1^2}.\end{aligned}$$

This concludes

$$\left\|\frac{\partial T\circ\tilde{\boldsymbol{\varphi}}_{n-1}}{\partial x_1}\right\|^2_{C(\Omega)} \le 4\overline{M}(\lambda_n\widetilde{M})^n$$

and

$$\left\|\frac{\partial^2 T\circ\tilde{\boldsymbol{\varphi}}_{n-1}}{\partial x_1^2}\right\|^2_{C(\Omega)} \le 6\overline{M}(\lambda_n\widetilde{M})^n.$$

Based on the above-mentioned discussion, we can get

$$\|H_1\|_{C(\Omega)} \le 10\overline{M}^2(\lambda_n\widetilde{M})^n.$$

In addition, we can also obtain the similar estimate for H_2, H_3. Therefore, we conclude

$$\|H(\sigma)\|_{C(\Omega)} \le \frac{10\overline{M}^2(\lambda_n\widetilde{M})^n}{(\kappa-\kappa_0)^2}.$$

Appendix B. Multigrid method for PDE (3.28). By adopting Grünwald approximation [41], $\frac{\partial^\alpha f(\mathbf{x})}{\partial x_i^\alpha}$, $\frac{\partial^{\alpha*} f(\mathbf{x})}{\partial x_i^{\alpha*}} (i=1,2)$ are discretized as follows:

$$\frac{\partial^\alpha f(\mathbf{x}_{p,q})}{\partial x_i^\alpha} = \delta_{i-}^\alpha f(\mathbf{x}_{p,q}) + O(h), \quad \frac{\partial^{\alpha*} f(\mathbf{x}_{p,q})}{\partial x_i^{\alpha*}} = \delta_{i+}^\alpha f(\mathbf{x}_{p,q}) + O(h), \tag{B.1}$$

where $\delta_{1-}^\alpha f_{p,q} = \frac{1}{h^\alpha}\sum_{l=0}^{p+1} \rho_l^{(\alpha)} f_{p-l+1,q}$, $\delta_{1+}^\alpha f_{p,q} = \frac{1}{h^\alpha}\sum_{l=0}^{N-p+2} \rho_l^{(\alpha)} f_{p+l-1,q}$, $\delta_{2-}^\alpha f_{p,q} = \frac{1}{h^\alpha}\sum_{m=0}^{q+1} \rho_m^{(\alpha)} f_{p,q-m+1}$, $\delta_{2+}^\alpha f_{p,q,r} = \frac{1}{h^\alpha}\sum_{m=0}^{N-q+2} \rho_m^{(\alpha)} f_{p,q+m-1}$, and $\rho_l^{(\alpha)}$ is computed by the formula $\rho_0^{(\alpha)} = 1$, $\rho_l^{(\alpha)} = (1 - \frac{1+\alpha}{l})\rho_{l-1}^{(\alpha)}$. Note that here, we use $f_{p,q}$ to denote $f(\mathbf{x}_{p,q})$ for any function f.

Let $U_q = (f_{1,q}, f_{2,q}, \ldots, f_{N,q})^T$; then it follows from (B.1) that

$$\frac{\partial^\alpha U_q}{\partial x_1^\alpha} \approx B_{N,\alpha} U_q, \quad \frac{\partial^{\alpha*} U_q}{\partial x_1^{\alpha*}} \approx B_{N,\alpha}^T U_q,$$

where $\frac{\partial^\alpha U_q}{\partial x_1^\alpha} = \left(\frac{\partial^\alpha f_{1,q}}{\partial x_1^\alpha}, \frac{\partial^\alpha f_{2,q}}{\partial x_1^\alpha}, \ldots, \frac{\partial^\alpha f_{N,q}}{\partial x_1^\alpha}\right)^T$, $\frac{\partial^{\alpha*} U_q}{\partial x_1^{\alpha*}} = \left(\frac{\partial^{\alpha*} f_{1,q}}{\partial x_1^{\alpha*}}, \frac{\partial^{\alpha*} f_{2,q}}{\partial x_1^{\alpha*}}, \ldots, \frac{\partial^{\alpha*} f_{N,q}}{\partial x_1^{\alpha*}}\right)^T$, and

$$B_{N,\alpha} = \frac{1}{h^\alpha} \begin{pmatrix} \rho_1^{(\alpha)} & \rho_0^{(\alpha)} & 0 & \cdots & 0 & 0 \\ \rho_2^{(\alpha)} & \rho_1^{(\alpha)} & \rho_0^{(\alpha)} & \cdots & 0 & 0 \\ \vdots & \vdots & \vdots & \ddots & \vdots & \vdots \\ \rho_{N-1}^{(\alpha)} & \rho_{N-2}^{(\alpha)} & \rho_{N-3}^{(\alpha)} & \cdots & \rho_1^{(\alpha)} & \rho_0^{(\alpha)} \\ \rho_N^{(\alpha)} & \rho_{N-1}^{(\alpha)} & \rho_{N-2}^{(\alpha)} & \cdots & \rho_2^{(\alpha)} & \rho_1^{(\alpha)} \end{pmatrix}.$$

Hence, we obtain

$$\frac{\partial^{\alpha*}}{\partial x_1^{\alpha*}} \left(\frac{\partial^\alpha U_q}{\partial x_1^\alpha}\right) = B_{N,\alpha}^T B_{N,\alpha} U_q \triangleq A_{N,\alpha} U_q.$$

In a similar way, we obtain the following two approximations for $\frac{\partial^{\alpha*}}{\partial x_2^{\alpha*}} \left(\frac{\partial^\alpha f(\mathbf{x})}{\partial x_2^\alpha}\right)$,

$$\frac{\partial^{\alpha*}}{\partial x_2^{\alpha*}} \left(\frac{\partial^\alpha V_p}{\partial x_2^\alpha}\right) = A_{N,\alpha} V_p,$$

where $V_p = (f_{p,1}, f_{p,2}, \ldots, f_{p,N})^T$. By adopting the Grünwald approximation, $\mathrm{div}^{\alpha*}(\nabla^\alpha \mathbf{u}_n^{k+1})$ and $\Delta \mathbf{u}_n^{k+1}$ are approximated by the following two formulas:

$$\left(\mathrm{div}^{\alpha*}(\nabla^\alpha u_{n,\beta}^{k+1})\right)_{p,q} \approx \sum_{l=0}^{N} \left(a_{N,\alpha}(p,l)(u_{n,\beta}^{k+1})_{l,q} + a_{N,\alpha}(q,l)(u_{n,\beta}^{k+1})_{p,l}\right) \tag{B.2}$$

and

$$\left(\Delta u_{n,\beta}^{k+1}\right)_{p,q} \approx \frac{1}{h^2}((u_{n,\beta}^{k+1})_{p+1,q} + (u_{n,\beta}^{k+1})_{p-1,q} + (u_{n,\beta}^{k+1})_{p,q+1} + (u_{n,\beta}^{k+1})_{p,q-1} - 4(u_{n,\beta}^{k+1})_{p,q}), \tag{B.3}$$

where $\beta = 1, 2$ and $a_{N,\alpha}(p,l)$ is the entry of matrix $A_{N,\alpha}$ at the intersection of the p_{th} row and l_{th} column.

Then based on (B.2) and (B.3), (3.28) is discretized as follows:

$$
\begin{aligned}
&(1+4\gamma_n+2\theta_n\mu(a_{N,\alpha}(p,p)+a_{N,\alpha}(q,q)))(u_{n,\beta}^{k+1})_{p,q}\\
&+2\theta_n\mu\sum_{l=1,l\neq p,q}^{N_S}\Big(a_{N,\alpha}(p,l)(u_{n,\beta}^{k+1})_{l,q}+a_{N,\alpha}(q,l)(u_{n,\beta}^{k+1})_{p,l}\Big)\\
&-\gamma_n\Big((u_{n,\beta}^{k+1})_{p+1,q}+(u_{n,\beta}^{k+1})_{p-1,q}+(u_{n,\beta}^{k+1})_{p,q+1}+(u_{n,\beta}^{k+1})_{p,q-1}\Big)=(v_{n,\beta}^{k+1})_{p,q},
\end{aligned}
\tag{B.4}
$$

where $\gamma_n=\frac{2\theta_n\Theta}{h^2}$. Further, (B.4) induces the following solver for (3.28),

(B.5)

$$
\begin{aligned}
(u_{n,\beta}^{k+1})_{p,q}^{(t+1)}=\frac{1}{\Upsilon_n}\Bigg((v_{n,\beta}^{k+1})_{p,q}&-2\theta_n\mu\sum_{l=1,l\neq p,q}^{N_S}\Big(a_{N,\alpha}(p,l)(u_{n,\beta}^{k+1})_{l,q}^{(t)}+a_{N,\alpha}(q,l)(u_{n,\beta}^{k+1})_{p,l}^{(t)}\Big)\\
&+\gamma_n\Big((u_{n,\beta}^{k+1})_{p+1,q}^{(t)}+(u_{n,\beta}^{k+1})_{p-1,q}^{(t)}+(u_{n,\beta}^{k+1})_{p,q+1}^{(t)}+(u_{n,\beta}^{k+1})_{p,q-1}^{(t)}\Big)\Bigg),
\end{aligned}
$$

where $\Upsilon_n=1+4\gamma_n+2\theta_n\mu(a_{N,\alpha}(p,p)+a_{N,\alpha}(q,q))$ and $t=0,1,2,\ldots$.

Algorithm B.1 2D multigrid algorithm for **u**-problem.

Initialization: $\mathbf{u}_n^{k+1,h}=\mathbf{u}_n^{k,h}$, $\mathbf{u}_{n,0}^{k+1,h}=\mathbf{u}_n^{k,h}+\mathbf{\Pi}$, $\mu>0$, $\bar{k}=0$, and maximum iteration times K.

while $\|\mathbf{u}_n^{k+1,h}-\mathbf{u}_{n,0}^{k+1,h}\|\geq\|\mathbf{\Pi}\|$ and $\bar{k}\leq K$, **do**

$\mathbf{u}_{n,0}^{k+1,h}=\mathbf{u}_n^{k+1,h}$.

Step 1. relax (B.5) with initial guess $\mathbf{u}_n^{k+1,h}$; compute residual error $\mathbf{r}_n^{k+1,h}$ on Ω^h;

Set $level=L$.

Step 2. restrict the residual error to Ω^H by using $\mathbf{r}_n^{k+1,H}=R_h^H\mathbf{r}_n^{k+1,h}$;

Set $level=level-1$, $H=2h$, and relax (B.5) by replacing $\mathbf{v}_n^{k+1}$ with $\mathbf{r}_n^{k+1,H}$, and with initial guess $\mathbf{u}_n^{k+1,H}=\mathbf{0}$ to obtain approximations $\bar{\mathbf{u}}_n^{k+1,H}$; update residual error $\mathbf{r}_n^{k+1,H}$;

Step 3.

if $level=1$,

do: accurately solve the system (B.5) by replacing $\mathbf{v}_n^{k+1}$ with $\mathbf{r}_n^{k+1,H}$ to obtain the solution $\mathbf{u}_n^{k+1,H}$;

else

do: repeat **Step 2** until $level=1$.

end if

Step 4.

if $level=L$,

do: relax (B.5) to obtain the final solution $\mathbf{u}_n^{k+1,h}$ for this round and let $\bar{k}=\bar{k}+1$;

else

do(repeat): interpolate the correction to next fine grid by letting $\mathbf{u}_{n,t}^{k+1,h}=I_H^h\mathbf{u}_n^{k+1,H}$; update current grid approximations using correction $\hat{\mathbf{u}}_n^{k+1,h}=\mathbf{u}_{n,t}^{k+1,h}+\bar{\mathbf{u}}_n^{k+1,h}$; relax (B.5) with initial guess $\hat{\mathbf{u}}_n^{k+1,h}$ on fine grid to obtain approximations $\mathbf{u}_n^{k+1,h}$ and let $level=level+1$. Repeat this process until $level=L$.

end if.

end while

Output: $\mathbf{u}_n^{k+1}=\mathbf{u}_n^{k+1,h}$.

To solve the algebraic system (B.4), many numerical techniques can be used, such as the Jacobi iteration, the Gauss–Seidel iteration, and the multigrid method. Here we choose the multigrid method to accelerate the Jacobi iterative technique. One round of V-cycle of the multigrid method contains four steps: Step 1. smoothing; Step 2. restriction; Step 3. coarsest grid solution; Step 4. interpolation. Since this technique is similar to the steps in [17, 20], we omit the introduction for these four steps and refer the reader to [17, 20] for details. However, to make our paper self-contained, based on (B.5), the multigrid algorithm for (3.28) can be summarized in Algorithm B.1.

Acknowledgments. The authors of this paper would like to thank Hang Li in Hospital of Stomatology, Wuhan University, for providing the data for Test II. Thanks also to the referees for their very helpful remarks.

REFERENCES

[1] M. Burger, J. Modersitzki, and L. Ruthotto, *A hyperelastic regularization energy for image registration*, SIAM J. Sci. Comput., 35 (2013), pp. B132–B148, https://doi.org/10.1137/110835955.

[2] A. Chambolle, *An algorithm for total variation minimization and applications*, J. Math. Imaging Vision, 20 (2004), pp. 89–97, https://doi.org/10.1023/B:JMIV.0000011325.36760.1e.

[3] C. Chen and O. Öktem, *Indirect image registration with large diffeomorphic deformations*, SIAM J. Imaging Sci., 11 (2018), pp. 575–617, https://doi.org/10.1137/17M1134627.

[4] Y. Chen, J. Shi, M. Rao, and J. Lee, *Deformable multi-modal image registration by maximizing Rényi's statistical dependence measure*, Inverse Probl. Imaging, 9 (2015), pp. 79–103, https://doi.org/10.3934/ipi.2015.9.79.

[5] G. Christensen, R. Rabbitt, and M. Miller, *Deformable templates using large deformation kinematics*, IEEE Trans. Image Process., 5 (1996), pp. 1435–1447, https://doi.org/10.1109/83.536892.

[6] N. Chumchob, *Vectorial total variation-based regularization for variational image registration*, IEEE Trans. Image Process., 22 (2013), pp. 4551–4559, https://doi.org/10.1109/TIP.2013.2274749.

[7] N. Chumchob, K. Chen, and C. Loeza, *A fourth-order variational image registration model and its fast multi grid algorithm*, Multiscale Model. Simul., 9 (2011), pp. 89–128, https://doi.org/10.1137/100788239.

[8] N. Debroux, C. Le Guyader, and L. A. Vese, *A multiscale deformation representation*, SIAM J. Imaging Sci., 16 (2023), pp. 802–841, https://doi.org/10.1137/22M1510200.

[9] F. Demengel, G. Demengel, and R. Erne, *Functional Spaces for the Theory of Elliptic Partial Differential Equations*, Springer, London, 2012.

[10] M. Droske and M. Rumpf, *A variational approach to nonrigid morphological image registration*, SIAM J. Appl. Math., 64 (2004), pp. 668–687.

[11] M. Ebrahimi and S. Kulaseharan, *Deformable image registration and intensity correction of cardiac perfusion MRI*, in Statistical Atlases and Computational Models of the Heart - Imaging and Modelling Challenges, Lecture Notes in Comput. Sci. 8896, Springer, New York, 2015, pp. 13–20, https://doi.org/10.1007/978-3-319-14678-2_2.

[12] M. Ebrahimi, A. Lausch, and A. L. Martel, *A Gauss-Newton approach to joint image registration and intensity correction*, Comput. Methods Prog. Biomed., 112 (2013), pp. 398–406, https://doi.org/10.1016/j.cmpb.2013.07.026.

[13] L. Evans, *Partial Differential Equations*, American Mathematical Society, Providence, RI, 2010.

[14] D. Ferreira, E. Ribeiro, and C. Barcelos, *A variational approach to non-rigid image registration with Bregman divergences and multiple features*, Pattern Recognit., 77 (2018), pp. 237–247, https://doi.org/10.1016/j.patcog.2017.12.015.

[15] E. Haber and J. Modersitzki, *A multilevel method for image registration*, SIAM J. Sci. Comput., 27 (2006), pp. 1594–1607, https://doi.org/10.1137/040608106.

[16] H. Han, *A variational model with fractional-order regularization term arising in registration of diffusion tensor image*, Inverse Probl. Imaging, 12 (2018), pp. 1263–1291.

[17] H. Han and A. Wang, *A fast multi grid algorithm for 2D diffeomorphic image registration model*, J. Comput. Appl. Math., 394 (2021), 113567, https://doi.org/10.1016/j.cam.2021.113576.

[18] H. Han and Z. Wang, *A diffeomorphic image registration model with fractional-order regularization and Cauchy-Riemann constraint*, SIAM J. Imaging Sci., 13 (2020), pp. 1240–1271, https://doi.org/10.1137/19M1260621.

[19] H. Han and Z. Wang, *3D diffeomorphic image registration with Cauchy-Riemann constraint and lower bounded deformation divergence*, ESAIM Math. Model. Numer., 57 (2023), pp. 299–328, https://doi.org/10.1051/m2an/2022080.

[20] H. Han, Z. Wang, and Y. Zhang, *Multiscale approach for two-dimensional diffeomorphic image registration*, Multiscale Model. Simul., 19 (2021), pp. 1538–1572, https://doi.org/10.1137/20M1383987.

[21] H. Han, Z. Wang, and Y. Zhang, *Multiscale approach for three-dimensional conformal image registration*, SIAM J. Imaging Sci., 15 (2022), pp. 1431–1468, https://doi.org/10.1137/21M1455929.

[22] C. Kanzow and Y. Shehu, *Strong convergence of a double projection-type method for monotone variational inequalities in hilbert spaces*, J. Fixed Point Theory Appl., 20 (2018), pp. 51–72.

[23] K. C. Lam and L. M. Lui, *Landmark and intensity based registration with large deformations via quasi-conformal maps*, SIAM J. Imaging Sci., 7 (2013), pp. 2364–2392, https://doi.org/10.1137/130943406.

[24] H. Li, W. Guo, J. Liu, L. Cui, and D. Xie, *Image segmentation with adaptive spatial priors from joint registration*, SIAM J. Imaging Sci., 15 (2022), pp. 1314–1344, https://doi.org/10.1137/21M1444874.

[25] J. Li, Y. Shi, G. Tran, I. Dinov, D. Wang, and A. Toga, *Fast local trust region for diffusion tensor registration using exact reorientation and regularization*, IEEE Tans. Med. Imaging, 33 (2014), pp. 1–43, https://doi.org/10.1109/TMI.2013.2274051.

[26] J. Liu, M. Yan, and T. Zeng, *Surface-aware blind image deblurring*, IEEE Trans. Pattern Anal. Mach. Intell., 43 (2021), pp. 1041–1055, https://doi.org/10.1109/TPAMI.2019.2941472.

[27] L. M. Lui and T. C. Ng, *A splitting method for diffeomorphism optimization problem using Beltrami coefficients*, J. Sci. Comput., 63 (2015), pp. 573–611, https://doi.org/10.1007/s10915-014-9903-4.

[28] F. Maes, A. Collignon, D. Vandermeulen, G. Marchal, and P. Suetens, *Diffeomorphic demons: Efficient non-parametric image registration*, IEEE Trans. Med. Imaging, 16 (1997), pp. 187–198, https://doi.org/10.1109/42.563664.

[29] K. Maleelai, C. Watchararuangwit, and N. Chumchob, *An improved numerical method for variational image registration model with intensity correction*, J. Interdiscip. Math., 25 (2022), pp. 1005–1022, https://doi.org/10.1080/09720502.2021.1889781.

[30] D. Qiu, K.-C. Lam, and L.-M. Lui, *Computing quasi-conformal folds*, SIAM J. Imaging Sci., 12 (2019), pp. 1392–1424, https://doi.org/10.1137/18M1220042.

[31] D. Qiu and L. M. Lui, *Inconsistent surface registration via optimization of mapping distortions*, J. Sci. Comput., 83 (2020), pp. 1–31, https://doi.org/10.1007/s10915-020-01246-5.

[32] E. Tadmor and L. V. S. Nezzar, *A multiscale image representation using hierarchical* (bv, l^2) *decompositions*, Multiscale Model. Simul., 2 (2004), pp. 554–579, https://doi.org/10.1137/030600448.

[33] A. Theljani and K. Chen, *A Nash game based variational model for joint image intensity correction and registration to deal with varying illumination*, Inverse Problems, 36 (2020), 034002, https://doi.org/10.1088/1361-6420/ab2934.

[34] T. Vercauteren, X. Pennecb, A. Perchanta, and N. Ayacheb, *Diffeomorphic demons: Efficient non-parametric image registration*, Neuroimage, 45 (2009), pp. 61–72, https://doi.org/10.1109/TMI.2016.2610583.

[35] R. Xu, P. Athavale, A. Nachman, and G. A. Wright, *Multiscale registration of real-time and prior MRI data for image-guided cardiac interventions*, IEEE Trans. Bio-Med. Eng., 61 (2014), pp. 2621–2632, https://doi.org/10.1109/TBME.2014.2324998.

[36] C. P. Yung, G. Choi, K. Chen, and L. M. Lui, *Efficient feature-based image registration by mapping sparsified surfaces*, J. Vis. Commun. Image R, 55 (2018), pp. 561–571, https://doi.org/10.1016/j.jvcir.2018.07.005.

[37] C. Zhang, W. Yang, X. Li, and H. Han, *MMGInpainting: Multi-modality guided image inpainting based on diffusion models*, IEEE Trans. Multimedia, 1 (2024), accepted, https://doi.org/10.1109/TMM.2024.3382484.

[38] D. Zhang and K. Chen, *A novel diffeomorphic model for image registration and its algorithm*, J. Math. Imaging Vision, 2018 (2018), pp. 1–30, https://doi.org/10.1007/s10851-018-0811-3.

[39] D. Zhang and K. Chen, *3D orientation-preserving variational models for accurate image registration*, SIAM J. Imaging Sci., 13 (2020), pp. 1653–1691, https://doi.org/10.1137/20M1320006.

[40] D. Zhang, G. P. T. Choi, J. Zhang, and L. M. Lui, *A unifying framework for n-dimensional quasi-conformal mappings*, SIAM J. Imaging Sci., 15 (2022), pp. 960–988, https://doi.org/10.1137/21M1457497.

[41] J. Zhang and K. Chen, *Variational image registration by a total fractional-order variation model*, J. Comput. Phys., 293 (2015), pp. 442–461, https://doi.org/10.1016/j.jcp.2015.02.021.

[42] J. Zhang, K. Chen, and B. Yu, *A novel high-order functional based image registration model with inequality constraint*, Comput. Math. Appl., 72 (2014), pp. 2887–2899, https://doi.org/10.1016/j.camwa.2016.10.018.